Equilibrium Theory-based Assessment of Dual-Reflux Pressure Swing Adsorption Cycles that Utilize Light Gas for Pressure Swing

[^]Tushar S. Bhatt, [†]Giuseppe Storti, [^]Joeri F. M. Denayer, [«]*Renato Rota

[^]Vrije Universiteit Brussel, Bioengineering Sciences Department, Pleinlaan 2, B-1050 Brussel, Belgium
[†]ETH Zurich, Institute of Chemical and Bioengineering, HCI F 125, Vladimir-Prelog-Weg 1-5/10, 8093 Zürich, Switzerland
[«]Politecnico di Milano, Department of Chemistry, Materials and Chemical Engineering, Via Mancinelli 7, I-20131 Milan, Italy

ABSTRACT: Binary gas mixtures can be completely separated via dual-reflux pressure swing adsorption (DR-PSA) process, where pressure of the column to which the feed gas is supplied and the kind of gas employed for pressure swing determine different configurations. DR-PSA studies have been predominantly confined to the configurations that use heavy gas for pressure swing. For such configurations, we formerly reported an equilibrium theory-based optimum design approach that defined a complete separation region and a selection criterion to enable the choice of suitable configuration. In this article, same design strategy is applied to the less studied DR-PSA configurations, those utilizing light gas for pressure swing. Unique understanding of the separation behavior of such configurations is achieved and presented. After discussing the impact of process variables on design constraints, a systematic analysis of key parameters defining the process performance with respect to the ratio of high to low operating pressures is finally reported.

AUTHOR INFORMATION
Corresponding Author
*Telephone: +39.02.2399.3154, Fax: +39.02.2399.3180, E-mail address: renato.rota@polimi.it

Notes
The authors declare no competing financial interest.

DOI: 10.1021/acs.iecr.8b04415

1. INTRODUCTION

Dual-reflux pressure swing adsorption (in the following referred to as DR-PSA) is an adsorption process technology that can be utilized for separating and/or purifying gaseous mixtures. It was put forth by Hirose[1] and concurrently patented by Leavitt[2], who denoted it as *duplex* PSA. In theory, DR-PSA process can obtain a complete separation of a binary feed gas blend into two pure products: one comprising of only the strongly adsorbed species (A) while the other comprising of only the feebly adsorbed species (B). A standard DR-PSA unit comprises of two identical adsorbent beds, each equipped with a provision for injecting the feed at position Z_F along its axial length. Z_F bifurcates each bed into *stripping* section (SS) and *rectifying* section (RS).

Each cycle of the DR-PSA process consists of several steps, some of which are executed at constant bed pressure while others are executed at non-constant bed pressures. During constant pressure steps: (i) feed is injected in the bed operational at constant high (P_H) or low pressure (P_L); (ii) light product (LP, constituted by pure B) and light reflux (LR, also constituted by pure B) are withdrawn from the SS end of the bed at constant P_H; (iii) heavy reflux stream (HR, constituted by pure A) as well as heavy product steam (HP, also constituted by pure A) are withdrawn from the RS end of the bed at constant P_L; (iv) light reflux (LR, constituted by pure B) is injected at the SS end of bed at constant P_L and; (v) heavy reflux stream (HR, constituted by pure A) is supplied to the RS end of bed at constant P_H. Alternatively, pressure swing is executed either with pure A (withdrawn from RS end of the bed undertaking depressurization) or with pure B (withdrawn from SS end of the bed undergoing depressurization) during non-constant pressure steps.

Two factors govern the sort of DR-PSA process cycle configuration: (i) the constant operating pressure (P_H or P_L) of the bed during which the feed gas is delivered to it, and; (ii) the type of gas (pure A or B) utilized for pressure swing. Accordingly, Kearns and Webley[3] identified four different DR-PSA process cycle configurations: (i) DR-PH-A: feed to the bed at P_H and A being utilized to achieve pressure swing; (ii) DR-PL-A: feed to the bed at P_L and A being utilized to achieve pressure swing; (iii) DR-PH-B: feed to the bed at P_H and B being utilized to achieve pressure swing, and; (iv) DR-PL-B: feed to the bed at P_L and B being utilized to achieve pressure swing. Even though binary feed gas mixture can be theoretically separated into two pure products by employing any of these configurations, literature survey[3-29] revealed that very few modeling and/or experimental studies have focused on the two cycle configurations that use pure light gas to achieve pressure swing (namely, DR-PL-B when feeding the bed at low pressure and DR-PH-B when feeding the bed at high pressure). Moreover, the motive behind such a bias was not clearly stated, the only exceptions being: Kearns and Webley[21], Bhatt et al.[22], Li et al.[11] and, May et al.[25]. Both, Kearns and Webley[21] and Bhatt et al.[22],

DOI: 10.1021/acs.iecr.8b04415

utilized the so-called equilibrium theory as solution approach[30] that assumes: zero resistance to mass transfer, perfect plug flow, ideal gas properties, negligible pressure drop, and isothermal conditions. Since such scenarios are seldom realized in practice, it is worthwhile mentioning that in real systems a complete separation can be not achieved even if the operating parameters are inside the range predicted by the equilibrium theory. Note that, Bhatt et al.[20, 22] have already particularized the advantages and limitations of utilizing the equilibrium theory for analysis of DR-PSA process in comparison with: actual experiments and detailed mathematical modeling approach. Kearns and Webley[21] proposed a productivity and energy consumption criterion, based on which a practicing engineer can select among the four process configurations mentioned above. However, their investigation did not aim at defining an optimum ratio between high to low operating pressures. Such restriction was overcome by Bhatt et al.[22] but their investigation was limited to DR-PL-A and DR-PH-A process configurations. Utilization of DR-PH-B configuration to separate N_2 and CO_2 feed gas mixture was experimentally demonstrated by Li et al.[11]. Mathematical modeling in Aspen Adsorption™ was also employed by the same authors[11] for optimizing the process performance. Nonetheless, the investigation of Li et al.[11] was limited to DR-PH-B configuration and separation of N_2 and CO_2 feed gas mixture. Recently, experimental demonstration of all the four DR-PSA process configurations was presented by May et al.[25] for separating N_2 and CH_4 using activated carbon. May et al.[25] also utilized non-isothermal Aspen Adsorption™ models for process optimization. Additionally, comparative assessment of all the four process cycle configurations was presented by May et al.[25] but, their results were restricted to the specific case N_2 and CH_4 separation using activated carbon.

Therefore, once more utilizing the equilibrium theory milieu for complete separation at cyclic steady state (CSS), in this work we extend our previous investigation to the two process cycle configurations that were less investigated in the literature, namely the ones using pure light gas to achieve pressure swing (DR-PL-B and DR-PH-B) while aiming to realize the following objectives:

(i) establish an optimum design methodology;

(ii) link Z_F to its range ($Z_{F,Min}$ to $Z_{F,Max}$);

(iii) study the effect of manipulating operating variable on process parameters;

(iv) propose an optimum range of the ratio between high and low operating pressures, and;

(v) give a support to the choice amongst all DR-PSA cycle configurations (namely: DR-PH-A, DR-PH-B, DR-PL-A, and DR-PL-B).

DOI: 10.1021/acs.iecr.8b04415

Note that the results derived from this work cannot be directly associated with the results derived by May et al. [25] because their analysis (via experimental data, theoretical calculations, and non-isothermal Aspen Adsorption™ models) was restricted to the specific case of incomplete separation of N_2 and CH_4 gas mixture using activated carbon in DR-PSA process configurations. Moreover, certain design and operating parameters like feed position, high to low operating pressure ratio, and adsorbent selectivity remained fixed throughout their[25] analysis. On the other hand, the forthcoming analysis via equilibrium theory assumes: complete separation of a two-components gas mixture (with unspecified components) with a flexible feed position in the in DR-PSA process, operating pressure ratio, and adsorbent selectivity.

2. DESCRIPTION OF PROCESS CYCLES

The schematic diagrams of typical twin-bed DR-PH-B and DR-PL-B process cycle configurations are shown in Fig. 1 and Fig. 2, respectively. The following statements apply to both configurations and/or their respective figures:

(i) perfect separation of a two-components gas mixture is assumed at CSS;

(ii) $Bed-I$ and $Bed-II$ are identical. Each of them undergo a cyclic process comprising of four steps: two steps are executed at constant pressure while the other two are executed at non-constant pressure;

(iii) only half-cycle is depicted because in the other half-cycle (not depicted here), same steps are carried out with the interchanged bed numbers;

(iv) the specific location along the length of the bed where binary feed gas mixture is injected is defined as Z_F. It is normalized axial coordinate ($Z = z/L_{bed}$) that splits each bed in two sections, namely, the *rectifying* section ($Z < Z_F; RS$) and the *stripping* section ($Z > Z_F; SS$);

(v) the bed end that remains closed during non-constant pressure steps is denoted as $Z = 0$ (This is consistent with the prior descriptions of other configurations of the DR-PSA process: DR-PH-A and DR-PL-A reported by Bhatt et al.[20] and Bhatt et al.[22], respectively. Moreover, in past representations of all DR-PSA configurations, pure B is either supplied-to or extracted-out of the *stripping* section, whereas pure A is either supplied-to or extracted-out of the *rectifying* section. Maintaining such consistency inevitably leads to reversal in location of *stripping* and *rectifying* sections in DR-PL-B and DR-PH-B when compared with that of DR-PL-A and DR-PH-A.);

(vi) Pure B ($y = 0$; y represents the mole fraction of heavy component) is either supplied-to or extracted-out of the end of SS, $Z = 1$, whereas pure A ($y = 1$) is either supplied-to or extracted-out of the end of RS, $Z = 0$.

DOI: 10.1021/acs.iecr.8b04415

2.1. DR-PH-B. A graphic representation of a standard DR-PH-B process cycle configuration is shown in Fig. 1. Binary feed gas (characterized by flowrate $\dot{N}_F$ and composition y_F) is supplied-to $Bed-I$ which is operated at constant high pressure (P_H) during the *feed* step (FE); at the same time, *purge* step (PU) is carried out in $Bed-II$ while being operated at constant P_L. Pure B $(y=0)$ is extracted from the $Bed-I$ at flowrate $\dot{N}_{H,out}$, a part of which is removed from the system as Light Product (LP) at flowrate $\dot{N}_F(1-y_F)$ and the residual part is provided as Light Reflux (LR) to $Bed-II$ (undergoing *purge* step) at flowrate $\dot{N}_{L,in}$. Pure A $(y=1)$ is extracted from $Bed-II$ at flowrate $\dot{N}_{L,out}$, a part of which is removed from the system as Heavy Product (HP) at flowrate $\dot{N}_F y_F$ and the residual part is compressed and injected-in $Bed-I$ as Heavy Reflux (HR) at flowrate $\dot{N}_{H,in}$.

Once the concurrent FE/PU steps are completed, the change of the bed pressures is realized via transfer of pure B from the *stripping* end of $Bed-I$ (after compression) to the $Z=1$ end of $Bed-II$: *blowdown* step is carried out in $Bed-I$ and its pressure drops from P_H to P_L and, at the same time, *pressurization* step is carried out in $Bed-II$ and its pressure increases from P_L to P_H. The overall quantities of gas pushed-out of $Bed-I$ and supplied-to $Bed-II$ during these non-constant pressure steps are labelled N_{BD} and N_{PR}, respectively.

2.2. DR-PL-B. A graphic representation of a standard DR-PL-B process cycle configuration is shown in Fig. 2. Binary feed gas (characterized by flowrate $\dot{N}_F$ and composition y_F) is supplied-to $Bed-I$ which is operated at constant low pressure (P_L) during the *feed* step (FE); at the same time, *purge* step (PU) is carried out in $Bed-II$ while being operated at constant P_H. Pure A $(y=1)$ is extracted-out of the $Bed-I$ at flowrate $\dot{N}_{L,out}$, a part of which is removed from the system as Heavy Product (HP) at flowrate $\dot{N}_F y_F$ and the residual part is compressed and provided as Heavy Reflux (HR) to $Bed-II$ (undergoing *purge* step) at flowrate $\dot{N}_{H,in}$. Pure B $(y=0)$ is extracted from $Bed-II$ at flowrate $\dot{N}_{H,out}$, a part of which is removed from the system as Light Product (LP) at flowrate $\dot{N}_F(1-y_F)$ and the residual part is injected-in $Bed-I$ as Light Reflux (LR) at flowrate $\dot{N}_{L,in}$.

When the concurrent FE/PU steps end, the change of bed pressures is realized via transfer of pure B from the *stripping* end of $Bed-II$ (after compression) to the $Z=1$ end of $Bed-I$. Due to this, *blowdown* step is carried out in $Bed-II$ and its pressure drops from P_H to P_L and, at the same time, *pressurization* step is carried out in $Bed-I$ and its pressure surges from P_L to P_H. The overall quantities of gas pushed-out of $Bed-II$ and supplied-to $Bed-I$ during these non-constant pressure steps are labelled as N_{BD} and N_{PR}, respectively.

DOI: 10.1021/acs.iecr.8b04415

3. EQUILIBRIUM THEORY-BASED MATHEMATICAL MODEL

Equilibrium theory-based mathematical model has already been described by Bhatt et al.[20]. That same mathematical model is employed in this article for the assessment of DR-PL-B and DR-PH-B configurations. Consequently, we retain: (i) all assumptions of the mathematical model, (ii) notations, descriptions, units and dimensions of all the variables and operating parameters, and (iii) governing equations of the mathematical model as reported by Bhatt et al.[20]. Hence, to avert reiteration, the equilibrium theory-based mathematical model is not described in this article.

4. MATHEMATICAL EVALUATION

Equilibrium theory-based mathematical model is employed to simulate one full cycle at which perfect separation of binary feed gas mixture is achieved in both DR-PL-B and DR-PH-B configurations at cyclic steady state (CSS). Two key demonstrations of such simulation of one full cycle will be put forth: (i) the column composition profiles with respect to time (depicted in Fig. 3 for DR-PH-B and Fig. 4 for DR-PL-B), and (ii) the illustration of various transitions and constant states of concentration in the space-time plane (represented in Fig. 5 for DR-PH-B and, Fig. 6 for DR-PL-B) i.e. the "topology" of the mathematical evaluation. In these depictions, the pressure and/or time evolutions along the length of the bed throughout one full cycle (comprising of four steps) are presented for just one bed; for complete separation at CSS, these representations are applicable to both beds. In Fig. 6 and Fig. 5, the y-axis i.e. the Cycle Time (t_{cycle}), is the duration of PU and FE (constant pressure) steps, while the same y-axis is the pressure during PR and BD (variable pressure) steps. Furthermore, each pressure or time interval has been normalized to the pressure change or to the duration of the step. Such normalization enabled us to realize identical size of the y-axis for each step of the process. Outlet and/or inlet molar flows $(\dot{N})$ and molar amounts (N) in Fig. 3 and Fig. 4 are indicated via arrows. To achieve complete separation at CSS, such molar flows and/or amounts should realize the subsequent conditions[20]:

Valid for *both* DR-PL-B and DR-PH-B configurations:

$$t_{FE} = t_{PU} \tag{1}$$

$$\dot{N}_{H,out} = \dot{N}_{L,in} + \dot{N}_F(1 - y_F) \tag{2}$$

$$\dot{N}_{L,out} = \dot{N}_{H,in} + \dot{N}_F y_F \tag{3}$$

$$N_{BD} = \frac{\varepsilon V_{bed}(P_H - P_L)}{RT\beta_B} = N_{PR} \tag{4}$$

Valid *only* for DR-PH-B configuration:

DOI: 10.1021/acs.iecr.8b04415

$$\dot{N}_{H,in} = \frac{\dot{N}_{L,in}}{\beta} - \dot{N}_F y_F \tag{5}$$

$$\dot{N}_{L,in} = \beta \dot{N}_{L,out} \tag{6}$$

Valid *only* for DR-PL-B configuration:

$$\dot{N}_{H,in} = \frac{\dot{N}_{H,out}}{\beta} \equiv \frac{\dot{N}_{L,in} + \dot{N}_F(1 - y_F)}{\beta} \tag{7}$$

$$\dot{N}_{L,in} = \beta \dot{N}_{L,out} - \dot{N}_F \mathbb{Y}(y_F) \tag{8}$$

where P_H (high pressure), P_L (low pressure), ε (adsorbent bed's interstitial porosity), V_{bed} (adsorbent bed volume), R (universal gas constant), T (operating temperature), β_i (affinity of the adsorbent towards component i; higher is the value, lower is the affinity, and vice versa), β (separation parameter of the adsorbent; since $\beta = \beta_A/\beta_B$, higher β value represents adsorbent with lower selectivity, and vice versa), y_F (mole fraction of heavy species in binary feed gas), t_{FE} (*feed* step duration) and t_{PU} (*purge* step duration) retain descriptions and dimensions identical to the ones reported by Bhatt et al.[20]. Consequently, in Eq. (8), $\mathbb{Y}(y_F) = 1 + (\beta - 1)y_F$. Having established the material balances, now we can tackle separately DR-PL-B and DR-PH-B process cycle configurations.

4.1. Equilibrium model for DR-PH-B process cycle configuration. In accordance to their mathematical formulations, the characteristics will form simple spreading waves during the *purge* (PU) and *pressurization* (PR) steps. In contrast, during *feed* (FE) and *blowdown* (BD) steps the characteristics will form self-sharpening waves (which may ultimately form shock waves). Therefore, $PU \rightarrow PR \rightarrow FE \rightarrow BD$ step sequence is followed to assess DR-PH-B process cycle.

To build the cycle illustrations in Fig. 3 and 5, the ultimate concentration profile that symbolizes the culmination of the *blowdown* step is used as initial concentration profile for the *purge* step. It comprises of two constant composition plateaus at $y = y^*$ and $y = 1$. A step-change at Z^* separates these two plateaus. The specific composition y^* can be evaluated at certain values of β, y_F, P_H and, P_L by utilizing the following equation:

$$\frac{y_F}{y^*} = \left(\frac{1 - y_F}{1 - y^*}\right)^{\beta} (\mathbb{P})^{\beta - 1} \tag{9}$$

here $\mathbb{P}$ is the ratio between high and low operating pressures stated as:

$$\mathbb{P} = \frac{P_H}{P_L} \tag{10}$$

Duration of the *purge* step (PU) is t_{PU} and it is operated at constant low pressure: $\dot{N}_{L,in}$ is supplied at $Z = 1$ with concentration $y = 0$ while, $\dot{N}_{L,out}$ with composition $y = 1$ gets pushed-out from $Z = 0$. These flows are interlinked via Eq. (6). A portion of $\dot{N}_{L,out}$ is removed from the system as pure heavy product (for complete separation at CSS, its

DOI: 10.1021/acs.iecr.8b04415

flow is equivalent to $\dot{N}_F y_F$) and the residual portion $\dot{N}_{H,in}$ is injected at $Z = 0$ end of the other bed as pure heavy recycle all through the high-pressure $feed$ step. Since PU is at constant pressure; using the molar flowrate $\dot{N}_{L,in}$ with composition $y = 0$ as reference[20], the following equation can be utilized to evaluate the trajectory of characteristics throughout the column:

$$-\frac{dZ}{d\theta}\Big|_C = \frac{\mathbb{C}}{\mathbb{Y}^2(y)} \tag{11}$$

where $\mathbb{Y}(y) = 1 + (\beta - 1)y$ and $\theta = t/t_{step}$. The negative sign in Eq. (11) is indicative of the reverse direction of gas flow during PU: from $Z = 1$ to $Z = 0$. The definition of the parameter $\mathbb{C}$, i.e. capacity ratio of the *purge* step, in Eq. (11) is equivalent to the one defined by Bhatt et al.[20], but restated here to avoid ambiguity.

$$\mathbb{C} = \frac{\beta_A \dot{N}_{L,in} t_{FE} RT}{P_L V_{bed} \varepsilon} \equiv \frac{\beta_A RT \mathbb{G}}{P_L \varepsilon} \frac{N_F}{V_{bed}} \tag{12}$$

Here the separation parameter of the adsorbent for species A is β_A and, pure light reflux to feed rate ratio is $\mathbb{G}$ as per the definition stated by Bhatt et al.[20]:

$$\mathbb{G} = \frac{\dot{N}_{L,in}}{\dot{N}_F} \tag{13}$$

The characteristic concentration remains constant while operating the system at constant pressure. Therefore, it is possible to integrate Eq. (11) and its integrated form is reported in Eq. (14):

$$(Z_0 - Z)|_y = \frac{\mathbb{C}}{\mathbb{Y}^2(y)} \tag{14}$$

Here Z and Z_0 describe the final and initial location of certain characteristic with composition (y). All through PU, the initial step at the rightmost location $Z = 1$ gets converted in a wave designated as *Stripping Wave* (SW). The concentration of SW remains identical all along the characteristics therefore, the ultimate right and left limiting mole fractions are $y = 0$ and $y = y^*$, respectively. At the termination of PU step, the ultimate location of y^* characteristic in SW can be assessed via Eq. (14):

$$Z^{PU}_{SW,y^*} = 1 - \frac{\mathbb{C}}{\mathbb{Y}^2(y^*)} \tag{15}$$

Such specific location has been expressed as Z^{PU}_{SW,y^*}: here the subscripts are the type of wave and the specific mole fraction respectively, and the superscript specifies the termination of the corresponding process step. Identical representation has been used for further distinct locations reported in Figs. 4, 6 and, 7.

DOI: 10.1021/acs.iecr.8b04415

All through PU, the initial step at the specific location $Z = Z^*$ spreads and gets converted in a wave designated as *Rectifying Wave* (RW). The concentration of RW remains identical all along the characteristics; therefore, the ultimate left and right limiting mole fractions are $y = 1$ and $y = y^*$, respectively. At the termination of the PU step, the ultimate location of y^* and $y = 1$ characteristic in RW can be again assessed via Eq. (14):

$$\left(Z^* - Z^{PU}_{RW,y^*}\right) = \frac{\mathbb{C}}{\mathbb{Y}^2(y^*)} \tag{16}$$

$$\left(Z^* - Z^{PU}_{RW,1}\right) = \frac{\mathbb{C}}{\beta^2} \tag{17}$$

All through the PR step (operated at non-constant pressures), the column end that remains closed is located in $Z = 0$. During PR, pure light gas amounting to N_{PR} moles is injected-in the bed (after compression) at $Z = 1$; due to this injection the pressure of the bed grows from the initial value of P_L to the ultimate value of P_H. This results in the shrinking of the concentration plateau initially at $y = y^*$ which reaches the final concentration value y_F. Likewise, the constant composition plateau characterized by pure A $(y = 1)$ shrinks as well, but its concentration value remains at $y = 1$. At the termination of PR step, the locations of the y_F and $y = 1$ characteristics can be computed via the equilibrium theory-based mathematical model[20] by utilizing the subsequent equations:

$$\frac{Z^{PU}_{SW,y^*}}{Z^{PR}_{SW,y_F}} = \mathbb{H} \tag{18}$$

$$\frac{Z^{PU}_{RW,y^*}}{Z^{PR}_{RW,y_F}} = \mathbb{H} \tag{19}$$

$$Z^{PU}_{RW,1} = Z^{PR}_{RW,1}(\mathbb{P}^{1/\beta}) \tag{20}$$

In Eq. (18) and (19), the description of $\mathbb{H}$ (a dimensionless term) remains equivalent to the one stated by Bhatt et al.[20], as reported in the following for the sake of clarity.

$$\mathbb{H} = \left(\frac{y^*}{y_F}\right)^{\beta/(1-\beta)} \left(\frac{1-y_F}{1-y^*}\right)^{1/(1-\beta)} \frac{\mathbb{Y}(y^*)}{\mathbb{Y}(y_F)} \tag{21}$$

The subsequent *feed* step (FE) has duration t_{FE} and it is operated at constant high pressure (P_H). Pure heavy reflux $\left(\dot{N}_{H,in}\right)$ is injected-in at $Z = 0$, $\dot{N}_F$ (having composition y_F) is injected-in at $Z = Z_F$, and pure light material $(y = 0)$ is pushed-out from the opposite end $(Z = 1)$ of the bed at flowrate $\dot{N}_{H,out}$. These flowrates are interlinked via Eq. (2) and (5). From every section of the bed, the inlet (in) and outlet (out) molar flows are stated below:

<u>*Stripping Section (SS)*:</u>

$$\dot{N}_{SS,in} = \frac{\dot{N}_{L,in} + \dot{N}_F(1-y_F)}{\mathbb{Y}(y_F)} \tag{22}$$

DOI: 10.1021/acs.iecr.8b04415

$$\dot{N}_{SS,out} = \dot{N}_{H,out} \tag{23}$$

Rectifying Section (RS):

$$\dot{N}_{RS,in} = \dot{N}_{H,in} \tag{24}$$

$$\dot{N}_{RS,out} = \frac{\beta \dot{N}_{H,in}}{\mathbb{Y}(y_F)} \tag{25}$$

During *feed* step (FE), self-sharpening waves are created by the converging characteristics. This may result in the development of shocks (S) in SW and/or RW, which of course depends on the operating conditions as well as the values of operating parameters. Yet again, the equilibrium theory-based mathematical model equations[3,20,30] can be used for a numerical assessment of the trajectory of characteristics and the propagation of shock waves formed through superposition of characteristics. In this work, numerical assessment for the development and propagation of shocks is based on direct check of the superposition of adjacent characteristics. Identical assessment technique was already employed by Bhatt et al.[20] and it is briefly reported in the Supporting Information. Particularly, if the development of shock occurs in the SW and/or RW, it will start only at their respective highest possible compositions: y_F and $y = 1$. This is due to the fact that the initial spreading of both SW and RW occurs during constant pressure PU which eradicates the possibility of introducing heterogeneity in both of these waves. The trajectories of shocks (S) and characteristics (C) should be assessed via the subsequent equations:

Stripping Section (SS):

$$\left.\frac{dZ}{d\theta}\right|_{SS,C} = \frac{\mathbb{C}}{\mathbb{Y}^2(y)}\left[1 + \frac{(1-y_F)}{\mathbb{G}}\right]\frac{1}{\mathbb{P}} \tag{26}$$

$$\left.\frac{dZ}{d\theta}\right|_{SS,S} = \frac{\mathbb{C}}{\mathbb{Y}(y_F)\mathbb{Y}(y_2)}\left[1 + \frac{(1-y_F)}{\mathbb{G}}\right]\frac{1}{\mathbb{P}} \tag{27}$$

Rectifying Section (RS):

$$\left.\frac{dZ}{d\theta}\right|_{RS,C} = \frac{\mathbb{C}}{\mathbb{Y}^2(y)}\left[1 - \frac{\beta y_F}{\mathbb{G}}\right]\frac{1}{\mathbb{P}} \tag{28}$$

$$\left.\frac{dZ}{d\theta}\right|_{RS,S} = \frac{\mathbb{C}}{\beta\mathbb{Y}(y_2)}\left[1 - \frac{\beta y_F}{\mathbb{G}}\right]\frac{1}{\mathbb{P}} \tag{29}$$

In Eq. (27) and (29), the subscript 2 refers to the concentration of the trailing edge of the shock wave. Moreover, in these equations, the composition of the leading edge of the shock has been replaced with the corresponding composition mentioned above.

A specific condition is shown in Fig. 3 and 5 where: (i) either shock formation *does not* occur in the RW throughout FE or, (ii) y_F characteristic at Z^{FE}_{RW,y_F} (the ultimate location of leftmost y_F characteristic at the culmination of FE) is

DOI: 10.1021/acs.iecr.8b04415

not engulfed by the shock developed in the RW. This situation is chosen to facilitate the discussion in the current section via simple equations. In either of these scenarios, the change in position of leftmost y_F characteristic during FE can be tracked using Eq. (28) as follows:

$$\left(Z^{FE}_{RW,y_F} - Z^{PR}_{RW,y_F}\right) = \frac{\mathbb{C}}{\mathbb{Y}^2(y_F)}\left[1 - \frac{\beta y_F}{\mathbb{G}}\right]\frac{1}{\mathbb{P}} \tag{30}$$

Eventually, let us consider the *blowdown* step (BD) during which the $Z = 0$ end of the bed remains shut. Pure light gas (amounting to N_{BD} moles) leaves the bed from $Z = 1$ and the pressure of the entire bed drops from the initial high pressure value (P_H) to the final low pressure one (P_L). Accordingly, the constant composition plateau with initial concentration of $y = y_F$, changes its concentration value up to $y = y^*$. Such circumstances result in self-sharpening waves due to converging characteristics which may eventually lead the development of shock (S) waves. Formation of shocks in SW and/or RW depends on the operating conditions as well as on the values of the operating parameters. On the other hand, if the shocks have already developed during the previous *feed* step, these shocks may develop and propagate further during the *blowdown* step. Yet again, the equilibrium theory-based mathematical model equations[3,20,30] can be used for a numerical assessment of the trajectory of characteristics and the propagation of shock waves formed through superposition of characteristics. Utilizing the composition profiles evaluated at the termination of the preceding step as initial wave profiles for the current step, the computation of the space-time propagations of both the transitions can accomplished. Moreover, the exact locations of shock formation and its complete development can also be determined via the same technique. Complete development of shock in the SW and RW is represented through small empty bullets in Fig. 5.

Therefore, the equilibrium theory-based mathematical model of the DR-PH-B process is summarized into the aforementioned equations which can be utilized for assessing the topology of the solution in each step. Considering complete separation at CSS for the DR-PH-B process, the aforementioned equations can be evaluated in a step by step sequence by utilizing the end conditions of one step as initial conditions for the subsequent step, to offer the comprehensive representation: composition-space-time. Final solution requires the values of the 7-subsequent adsorbent and/or design and/or operating parameters: concentration of heavy component in the binary feed gas mixture (y_F), parameter that governs the separation efficiency of the adsorbent (β), location of the RW at the start of the process cycle (Z^*), ratio between high and low pressure values ($\mathbb{P}$), light recycle to feed ratio ($\mathbb{G}$), capacity ratio of the *purge* step ($\mathbb{C}$) and, feed location (Z_F).

DOI: 10.1021/acs.iecr.8b04415

Note that, to realize the complete separation of a two-component feed gas at CSS for specific values of β, y_F, $\mathbb{G}$, $\mathbb{C}$, and $\mathbb{P}$, the value of Z_F and Z^* depend on one to another. In other words, when the value of anyone of these locations (for example, Z^*) gets computed, the value of the other location (Z_F) gets fixed by the constraint of perfect separation at CSS. Such a relationship between Z^* and Z_F is discussed in the subsequent subsection.

4.2. Optimum solution for DR-PH-B process cycle configuration - Triangular Operating Zone ($\boldsymbol{TOZ}$). To achieve a complete separation of two-components gas mixture at CSS, for specific values of concentration of heavy component in binary feed gas mixture (y_F), ratio between high and low operating pressure values ($\mathbb{P}$), and parameter that governs the separation efficiency of the adsorbent (β); the residual 4 process variables (Z_F, $\mathbb{G}$, $\mathbb{C}$ and, Z^*) need to be computed. Considering the topology of the solution presented in Fig. 5, three major locations that govern the separation are: $Z^{PR}_{RW,1}$, Z^{PR}_{SW,y_F} and, Z^{FE}_{RW,y_F}. To realize the perfect separation of a binary feed gas mixture, the values of these locations in addition to the values of locations of the *Stripping* and *Rectifying* waves at the beginning of the process cycle must satisfy the subsequent restraints:

1) Location value of the y_F characteristic in the *stripping* wave at the termination of PR step should not be less than the value of location at which the feed is injected-in the bed $\left(Z^{PR}_{SW,y_F} \geq Z_F\right)$. This will guarantee feed injection inside a constant composition plateau having concentration y_F thereby avoiding any modification in its concentration.
2) The leftmost characteristic of the RW having composition $y = 1$ at the termination of PR step should not leave the bed. Hence, its ultimate location, $Z^{PR}_{RW,1}$, should not be smaller than 0 ($Z^{PR}_{RW,1} \geq 0$). This will avoid the violation of the assumption of perfect separation of binary feed gas mixture at CSS conditions.
3) Location value of the y_F characteristic in the *rectifying* wave when the FE step ends should not exceed the value of the location at which feed is injected in the bed $\left(Z^{FE}_{RW,y_F} \leq Z_F\right)$. This will again guarantee feed injection inside a constant composition plateau having concentration y_F thereby avoiding any modification in its concentration.
4) Both the *rectifying* and *stripping* waves should "shrink" into completely developed shocks at the termination of *blowdown* step (SW: $y_1 = y^*, y_2 = 0$; RW: $y_1 = 1, y_2 = y^*$). Moreover, at the termination of *blowdown* step, SW must be at $Z = 1$ and the RW must be at Z^*. This will ensure that the composition profile considered as initial condition for the PU step is actually realized.

DOI: 10.1021/acs.iecr.8b04415

All of these requirements are utilized to assess possible values of light recycle to feed ratio ($\mathbb{G}$), feed location (Z_F), location of the RW at the start of the process cycle (Z^*), and capacity ratio of the *purge* step ($\mathbb{C}$). Note that the conditions mentioned above can be satisfied by a unique value of $\mathbb{G}$ and an array of values of Z_F, Z^* and, $\mathbb{C}$. Such a convenient property was also highlighted and discussed by Bhatt et al.[20]. Additionally, the value of $\mathbb{H}$ depends only on the values of the input parameters: $\mathbb{P}$, β, and y_F (cf. Eq. (9), (10), and (21)). Hence, for every $(\mathbb{C}, Z_F, Z^*)$ values that guarantee perfect separation of a given binary feed gas mixture at CSS, a unique value of $\mathbb{H}$ ~~is~~ arises.

Considering the typical constraints and characteristics mentioned above for realizing the perfect separation of a two-components feed gas mixture, the following iterative technique allows for evaluating the $\mathbb{G}, \mathbb{C}, Z_F$, and Z^* values:

(i) An initial value of $\mathbb{G}$ is assumed.

(ii) An operating region within the three-dimensional space ($\mathbb{C}, Z_F$ and Z^*) is determined. Perfect separation can be realized for every set of $\mathbb{C}, Z_F$ and Z^* that exists within such an operating region. Note that each of such set will result in a different value of the separation efficiency. In other words, each of such set will require different adsorbent quantities.

(iii) DR-PH-B process cycle is completely simulated by utilizing these values of $\mathbb{G}, \mathbb{C}, Z_F$ and Z^*. When perfect separation is realized at cyclic steady state conditions, the initially assumed value of $\mathbb{G}$ is considered to be correct. Conversely, when perfect separation is not realized, another value of $\mathbb{G}$ is guessed and the iterative process is repeated.

For the identification of the three-dimensional operating region, Eq. $(15) - (20)$ and (30) can be utilized as follows:

$$Z_{SW,y_F}^{PR} \equiv \frac{1}{\mathbb{H}}\left[1 - \frac{\mathbb{C}}{\mathbb{Y}^2(y^*)}\right] \geq Z_F \tag{31}$$

$$Z_{RW,1}^{PR} \equiv \frac{1}{(\mathbb{P}^{1/\beta})}\left[Z^* - \frac{\mathbb{C}}{\beta^2}\right] \geq 0 \tag{32}$$

$$Z_{RW,y_F}^{FE} \equiv \left[\frac{\mathbb{C}}{\mathbb{Y}^2(y_F)}\left(1 - \frac{\beta y_F}{\mathbb{G}}\right)\frac{1}{\mathbb{P}}\right] + \left[\frac{1}{\mathbb{H}}\left(Z^* - \frac{\mathbb{C}}{\mathbb{Y}^2(y^*)}\right)\right] \leq Z_F \tag{33}$$

At a certain value of the parameter $\mathbb{G}$, the three-dimensional (tetrahedral) operating region can be determined with $\mathbb{C}, Z_F$ and Z^* variables.

Utilizing the equality in Eq. (32): $Z^* = (\mathbb{C}/\beta^2)$, constraint (33) can be re-written as:

$$Z_{RW,y_F}^{FE} \equiv \mathbb{C}\left\{\left[\frac{1}{\mathbb{Y}^2(y_F)}\left(1 - \frac{\beta y_F}{\mathbb{G}}\right)\frac{1}{\mathbb{P}}\right] + \left[\frac{1}{\mathbb{H}}\left(\frac{1}{\beta^2} - \frac{1}{\mathbb{Y}^2(y^*)}\right)\right]\right\} \geq Z_F \tag{34}$$

Through Eq. (34), the operating region within the two-dimensional space $(Z_F, \mathbb{C})$ gets determined. Since it shows a triangular shape, it will be called 'Triangular Operating Zone' (TOZ). Both the inclined sides of the TOZ are *straight*

DOI: 10.1021/acs.iecr.8b04415

lines determined via inequalities (31) and (34) at their limits. A qualitative representation of such a region is shown in Fig. 7. Such a TOZ was formerly derived by Bhatt et al.[20] and Bhatt et al.[22] for DR-PH-A and DR-PL-A configuration, respectively.

Capacity ratio of the *purge* step ($\mathbb{C}$) determines the optimality of the process since it is proportional to the N_F/V_{bed} value within the TOZ. Therefore, at higher values of $\mathbb{C}$ the amount of feed that can be processed by a given bed volume is higher and/or the required amount of adsorbent for processing a given amount of feed is lower.

It is evident from Fig. 7 that the optimum operating condition can be derived from the top vertex of the TOZ which results from the intersection of the two straight lines derived from (31) and (34). Optimum feed injection position and maximum capacity ratio of the *purge* step come from the subsequent equations:

$$Z_{F,opt} = \left[\frac{1}{\mathbb{Y}^2(y^*)}\left\{\left[\frac{1}{\mathbb{Y}^2(y_F)}\left(1-\frac{\beta y_F}{\mathbb{G}}\right)\frac{1}{\mathbb{P}}\right]+\left[\frac{1}{\mathbb{H}}\left(\frac{1}{\beta^2}-\frac{1}{\mathbb{Y}^2(y^*)}\right)\right]\right\}^{-1}+\mathbb{H}\right]^{-1} \tag{35}$$

$$\mathbb{C}_{Max} \equiv \mathbb{Y}^2(y^*)\left[1-\mathbb{H}Z_{F,opt}\right] = Z_{F,opt}\left\{\left[\frac{1}{\mathbb{Y}^2(y_F)}\left(1-\frac{\beta y_F}{\mathbb{G}}\right)\frac{1}{\mathbb{P}}\right]+\left[\frac{1}{\mathbb{H}}\left(\frac{1}{\beta^2}-\frac{1}{\mathbb{Y}^2(y^*)}\right)\right]\right\}^{-1} \tag{36}$$

When the optimum conditions are considered (peak of the triangular operating zone): $Z^{PR}_{RW,1}=0$, $Z^{PR}_{SW,y_F}=Z^{FE}_{RW,y_F}=Z_{F,opt}$, and, through (32), $Z^*=(\mathbb{C}_{Max}/\beta^2)$.

It is again imperative to note here that the value of $Z_{F,opt}$ can be computed using Eq. (35) only in scenarios where: (i) either *no* shock develops in the RW during FE, or (ii) y_F characteristic at Z^{FE}_{RW,y_F} (the last location of leftmost y_F characteristic when the FE step ends) is not engulfed by the shock developed in the RW. On the other hand, when such scenarios don't exist (i.e. when leftmost y_F characteristic is engulfed by a shock during FE), the value of Z^{FE}_{RW,y_F} needs to be numerically evaluated by utilizing the equations mentioned in the previous section. Our detailed analysis has also revealed that, whether Z^{FE}_{RW,y_F} needs numerical or analytical evaluation, the resulting TOZ is: (i) delimited by two *straight* lines on its either sides, and (ii) the maximum ($Z_{F,Max}$) and minimum ($Z_{F,Min}$) limits of Z_F remain identical to the one depicted in Fig. 7.

4.3. Optimum solution for DR-PL-B process cycle configuration - Triangular Operating Zone (TOZ). Using the same procedure laid down in sections 4.1 and 4.2 for DR-PH-B process, the equilibrium model and TOZ for DR-PL-B process cycle configuration are evaluated. While the mathematical details of such an evaluation are outlined in the Supporting Information, the graphical representations are presented in Figures 6 to 8. Accordingly, for DR-PL-B configuration: (i) Fig. 4 represents the column composition profiles, (ii) Fig. 6 represents various transitions and constant states of

DOI: 10.1021/acs.iecr.8b04415

concentration in space and time, and (iii) graphical representation of the complete separation region is shown in Fig. 8.

4.4. Common conclusions about the optimal solution of DR-PH-B and DR-PL-B process cycle configurations.

Capacity ratio of the *purge* step $(\mathbb{C})$ bears direct proportionality to N_F/V_{bed} at constant β, $\mathbb{P}$, and y_F. Therefore, the least quantity of adsorbent will be needed for perfect separation of feed gas mixture when the process is operated at $\mathbb{C}_{Max}$. Such a corollary facilitates the assessment of the maximum quantity of feed gas mixture $(N_{F,Max})$ that can be perfectly separated when the system is operated at $\mathbb{C}_{Max}$ and $Z_{F,opt}$:

$$N_{F,Max} = \frac{P_L V_{bed} \varepsilon}{\beta_A RT} \frac{\mathbb{C}_{Max}}{\mathbb{G}} \tag{37}$$

The main features of the TOZ of DR-PL-B and DR-PH-B can be summarized as follows:

1) When increasing the capacity ratio of the *purge* step, the range of available feed injection locations reduce.
2) Optimum operating conditions are realized at the vertex of the TOZ where Z_F is equal to $Z_{F,opt}$ and $\mathbb{C}$ is equal to $\mathbb{C}_{Max}$.
3) The complete separation region is triangular (subsequently denoted as TOZ, i.e., Triangular Operating Zone).
4) Such TOZ unambiguously links the unique value of Z_F (as reported by Kearns and Webley[3]) to its minimum $(Z_{F,Min})$ and maximum $(Z_{F,Max})$ value (which is analogous to the suggestion of Ebner and Ritter[19] for realizing perfect separation of binary feed gas mixture in DR-PL-A cycle configuration).
5) By putting $\mathbb{C} = 0$ in: (i) Eq. (31) and (34) for DR-PH-B and (ii) Eq. $(S.12)$ and $(S.13)$ for DR-PL-B; the upper and lower limits of Z_F can be determined.
6) Within the TOZ there exists a unique value of both $\mathbb{H}$ and $\mathbb{G}$.
7) Perfect separation at CSS can be obtained while operating the system at any legitimate $(Z_F - \mathbb{C})$ combination selected inside the TOZ. Nevertheless, maximum adsorbent utilization can only be realized while operating the system at $\mathbb{C}_{Max}$ and $Z_{F,opt}$.
8) Complete separation at CSS can never be realized while operating the system at any $(Z_F - \mathbb{C})$ values outside the TOZ.

It is imperative to note here that the optimum operating conditions require a unique feed position. This situation will be difficult to be realized in practice since such an optimum feed position will fluctuate with variation in the operating conditions. To enhance the operational robustness of the process, an array of feed locations will be needed. It is

DOI: 10.1021/acs.iecr.8b04415

evident from Fig. 7 (for DR-PH-B) and Fig. 8 (for DR-PL-B) that such flexibility can be accomplished when a certain quantity of adsorbent remains unutilized.

5. RESULTS AND DISCUSSION

5.1. Performance of the process for various operating conditions within the TOZ. Triangular operating zone at certain $\mathbb{P}$, y_F, and β can be determined for DR-PL-B and DR-PH-B process cycle configurations. To demonstrate the optimal design approach, feasible $(Z_F - \mathbb{C})$ combinations can be selected from such TOZs and simulations can be performed via the numerical code briefly discussed in the Supporting Information. This analysis is fully analogous to the one previously reported by Bhatt et al.[20, 22] and, therefore, the corresponding results are reported in the Supporting Information.

5.2. Effect of input parameters on operating and design variables. For both DR-PH-B and DR-PL-B cycle configurations, the influence of $\mathbb{P}$, y_F, and β (input parameters) on $\mathbb{G}$ and $Z_{F,opt}$ (operating and design variables) is discussed in this section. Note that in this discussion, only maximum adsorbent utilization and perfect separation at CSS conditions are taken into consideration. Moreover, to facilitate comparative assessment, the boundaries of the axes remain identical in Fig. 9 and 10.

Simulations were carried out by changing $\mathbb{P}$ (from a lower limit to the upper limit of 10), at various values of y_F (from 0.1 to 0.9) and β. Enforcing the condition of complete shock development in the SW when the cycle ends governed the lower limit of $\mathbb{P}$. The simulations carried out at the lower β values (0.1 and 0.3) either failed to converge (because of incomplete shock development in the SW at the termination of the cycle since, if selectivity is extremely high, it may become impossible to regenerate the column during the PU/BD steps) or converged at $\mathbb{P}$ range that varied drastically for each process cycle configuration. Such simulation outcomes did not facilitate a clear comparative study. Therefore, only the simulation outcomes at β equal to 0.5, 0.7 and 0.9 are discussed here. Note that the adsorbents with the higher selectivity are characterized by lower β values (0.1 and 0.3), and feed gas mixture can be separated at such conditions but, in the majority of such scenarios, perfect separation is not achievable.

For DR-PL-B and DR-PH-B configurations, the change in $Z_{F,opt}$ with respect to $\mathbb{P}$ (at various β and y_F values) is presented in Fig. 9. For DR-PH-B configuration, the $Z_{F,opt}$ values move away from pure B $(Z = 1)$ end of the bed as the values of $\mathbb{P}$ increase, while for DR-PL-B configuration, the $Z_{F,opt}$ values come closer to pure B $(Z = 1)$ end of the bed as the values of $\mathbb{P}$ increase. Such trend of $Z_{F,opt}$ with respect to $\mathbb{P}$ for DR-PL-B configuration found in this work is consistent with the one reported by Kearns and Webley[21]. However, the trend of $Z_{F,opt}$ with respect to $\mathbb{P}$ for DR-PH-

DOI: 10.1021/acs.iecr.8b04415

B configuration found in this work is not consistent with the one reported by Kearns and Webley[21]. Our trend can also be understood by considering larger value of high to low operating pressure ratio ($\mathbb{P}$) in Figs. 3 and 4, inevitably resulting in the so-evaluated Z_F being closer to $Z = 0$ as compared to currently represented Z_F in the same figures. After much deliberation and thorough scrutiny, we inferred that the trend of $Z_{F,opt}$ with respect to $\mathbb{P}$ for DR-PH-B configuration presented in this work is unambiguous. For both DR-PL-B and DR-PH-B configurations, the influence of y_F on $Z_{F,opt}$ reduces with increase in β. To conclude with respect to the optimal feed position, operating the process at lower $\mathbb{P}$ is more practical for both DR-PH-B and DR-PL-B configurations. Here, practicality is defined in accordance with the criterion outlined by Kearns and Webley[21]. $Z_{F,opt}$ values that are either more than 5% or less than 95% of the bed length are deemed to be practical (consequently $Z_{F,opt} < 0.05$ and $Z_{F,opt} > 0.95$ are impractical values).

For DR-PL-B and DR-PH-B configurations, the variation of $\mathbb{G}$ with respect to $\mathbb{P}$ (for similar array of y_F and β values considered in Fig. 9) is depicted in Fig. 10. The y-axis of every chart is restricted to $\mathbb{G} = 50$ for better interpretation of the data. It is evident that $\mathbb{G}$ is inversely proportional to $\mathbb{P}$. Moreover, $\mathbb{G}$ is quite sensitive to smaller $\mathbb{P}$ values. Such sensitivity increases for adsorbents with higher β value (lower selectivity). This confirms the well-established notion that: high recycle ratios are required for adsorbents with lower selectivity when the same process performance needs to be achieved at certain $\mathbb{P}$ and y_F values.

5.3. Comparative assessment of all DR-PSA process cycle configurations. Kearns and Webley[21] have already highlighted the importance of pressure equalization step in reducing the energy needed for compression of gases in DR-PSA process operation. To realize pressure equalization in both DR-PH-B and DR-PL-B process cycle configurations (cf. Kearns and Webley[21]), equalization valve is utilized to connect the light gas ends of both the columns, from the beginning of PR or BD until equalization pressure $\left(P_{Eq}\right)$ is attained. Consequently, the real quantity of gas that needs to be compressed to attend the pressure swing is the gas pushed-out of the column undergoing BD solely when its pressure drops from P_{Eq} to P_L. In order to maintain consistency with our previous work, the definition of equalization pressure is held identical to the one used by Bhatt et al.[22]:

$$P_{Eq} = \left(\frac{P_H + P_L}{2}\right) \tag{38}$$

The type (pure B: $y = 0$) and number of moles ($N_{PR} \equiv N_{BD}$) of gas that is required to be transferred from one bed to the other for realizing the pressure swing in DR-PH-B and DR-PL-B configurations is identical (cf. Eq. (4)). Such opportune coincidence (in combination with the assumption of linear adsorption isotherms) facilitates us to infer the real amount of gas that needs to be compressed ($Comp$) for accomplishing the Pressure Swing (PS):

DOI: 10.1021/acs.iecr.8b04415

$$N_{Comp,PS} = \frac{\varepsilon V_{bed}\left(P_H - P_{Eq}\right)}{RT\beta_B} \equiv \frac{N_{PR}}{2} \tag{39}$$

Additionally, the gas that requires compression energy in DR-PH-B and DR-PL-B configurations is: $N_{H,in}$ (cf. Fig. 1 and 2). Considering perfect separation of $N_{F,Max}$ in DR-PL-B and DR-PH-B configurations and employing identical definition of $\mathbb{G}$, $N_{H,in}$ can be computed via the subsequent equations:

For DR-PH-B configuration:

$$N_{H,in} = \left[\left(\frac{\mathbb{G}}{\beta}\right) - y_F\right] N_{F,Max} \tag{40}$$

For DR-PL-B configuration:

$$N_{H,in} = \left[\frac{\mathbb{G} + (1 - y_F)}{\beta}\right] N_{F,Max} \tag{41}$$

Consequently, in DR-PL-B and DR-PH-B configurations, the quantity of gas that is required to be compressed ($Comp$) is equivalent to the sum of: (i) the real quantity of gas that needs to be compressed for accomplishing the pressure swing and, (ii) the quantity of gas utilized as heavy reflux:

$$N_{Comp} = \left(N_{Comp,PS} + N_{H,in}\right) \tag{42}$$

Note that the definition of $\mathbb{G}$ and N_{Comp} considered in this article is equal to the one employed by Bhatt et al.[22] (for DR-PL-A configuration) and Bhatt et al.[20] (for DR-PH-A configuration).

It is also worthwhile noting that, even for the same values of P_L, $\mathbb{P}$, V_{bed}, ε, β_A, β, R, T, and y_F; the calculated values of $Z_{F,opt}$, $\mathbb{G}$, and $\mathbb{C}_{Max}$ (and therefore the values $N_{F,Max}$, $N_{H,in}$, and N_{Comp}) for all four DR-PSA process cycle configurations will not be identical. This can enable the choice between all the four DR-PSA process cycle configurations.

For each DR-PSA process cycle configurations, $N_{F,Max}$ (maximum quantity of feed that can be processed) and N_{Comp} (total quantity of gas that needs to be compressed) can be computed by assuming: (i) perfect separation of feed gas mixture at CSS, (ii) optimal operating conditions ($\mathbb{C}_{Max}$ and $Z_{F,opt}$), (iii) complete utilization of the adsorbent, (iv) identical type of adsorbent, quantity of adsorbent, composition of feed gas, operating temperature and pressure ratio. The consequent ratio $N_{F,Max}/N_{Comp}$ can be used for the selection of appropriate process cycle configuration. Higher values of this ratio suggest that higher quantity of feed can be completely separated $\left(N_{F,Max}\right)$ at lower expense of energy (since a lower quantity of gas needs to be compressed, N_{Comp}).

DOI: 10.1021/acs.iecr.8b04415

To support the choice amongst different process cycle configurations, the quantities N_{Comp} and $N_{F,Max}$ were evaluated (for DR-PL-B and DR-PH-B in this work and for DR-PL-A and DR-PH-A by Bhatt et al. [22]) at identical P_L, V_{bed}, ε, β_A, R, and T, and at optimal operating conditions ($\mathbb{C}_{Max}$ and $Z_{F,opt}$). In particular, we used the values of P_L, V_{bed}, ε, β_A, R, and T reported by Kearns and Webley[21]. However, if some other values of these parameters would have been selected, the resulting N_{Comp} and $N_{F,Max}$ would have differed values but their ratio $\left(N_{F,Max}/N_{Comp}\right)$ computed at certain $\mathbb{P}$, β and y_F will remain equal to the ones reported in this article.

The ratio $N_{F,Max}/N_{Comp}$ at different $\mathbb{P}$, β, and y_F is presented in Fig. 11 for DR-PL-B and DR-PH-B. This figure can be directly compared with the analogous figure reported by Bhatt et al.[22] for DR-PL-A and DR-PH-A. Yet again, to facilitate comparative assessment, the boundaries of the axes have been kept identical. Since the trends at $y_F = 0.1$ and $y_F = 0.3$ in DR-PL-B and DR-PH-B are very different with respect to all other cases, we will neglect them to generalize the assessment of the current section. In each of these charts, the ratio $\left(N_{F,Max}/N_{Comp}\right)$ follows a certain trend when increasing the $\mathbb{P}$ values: sharp surge (in the beginning) followed by a smooth decline due to two contradictory influences: (i) the decline of $\mathbb{G}$ when increasing $\mathbb{P}$ (cf. Fig. 10) and (ii) the relationship between $\mathbb{P}$ and $N_{Comp,PS}$ requiring higher quantity of gas to be compressed at higher operating pressure ratios. As per the definition of light recycle ratio $\left(\mathbb{G} = \dot{N}_{L,in}/\dot{N}_F\right)$, lower $\mathbb{P}$ values result in higher $\dot{N}_{L,in}$ (and consequently higher $N_{H,in}$) and/or lower N_F, and vice versa. The calculated values of $N_{F,Max}/N_{Comp}$ exhibit a peak at specific value of $\mathbb{P}$, which will be termed "optimal operating pressure ratio": for each curve such value falls within the shaded region of the graphs presented in Fig. 11 (and in the analogous figure reported by Bhatt et al.[22] for DR-PL-A and DR-PH-A).

From the results presented in the figures, the subsequent guiding principles can be deduced:

(1) In all four DR-PSA systems, utilization of higher selectivity (smaller β value) adsorbents results in higher quantity of feed gas mixture that can be completely separated at lower energy consumption. This is because it has been observed that, in all four DR-PSA process cycle configurations: at any $\mathbb{P}$, the value of $\mathbb{G}$ increases (subsequently $N_{H,in}$ increases and/or N_F decreases) at increasing value of β.

(2) When pressure swing needs to be carried out with heavy gas, DR-PL-A system must be chosen (instead of a DR-PH-A system) uniquely when feed mixtures with $y_F \geq 0.9$ needs to be completely separated. Therefore, for $y_F < 0.9$, DR-PH-A should be chosen when operating the system at lower $\mathbb{P}$.

(3) When pressure swing needs to be carried out with light gas, DR-PL-B system must be chosen (instead of a DR-PH-B system) uniquely when feed gas with $y_F \geq 0.9$ needs to be completely separated.

DOI: 10.1021/acs.iecr.8b04415

(4) DR-PSA systems that accomplish pressure swing via pure light gas (DR-PL-B and DR-PH-B) are capable of processing higher quantity of feed gas at lower consumption of energy when compared with DR-PSA systems that accomplish pressure swing via pure heavy gas (DR-PL-A and DR-PH-A).

Almost all these conclusions are consistent with those discussed by May et al.[22]; some partial disagreements are not surprising if we consider that the conditions investigated by May et al.[22] are very different from those allowing the use of the equilibrium theory presented in this article, invariably assuming complete separation. Moreover, it should be noted that, when pressure swing needs to be carried out with light gas (DR-PH-B and DR-PL-B configurations), two separate compressors are needed in practice. This is because streams with two totally opposite compositions need to be compressed in DR-PL-B and DR-PH-B configurations: (i) pure heavy $(y = 1)$ recycle stream $\left(\dot{N}_{H,in}\right)$, to be pushed-in the bed operated at constant P_H, and (ii) pure B $(y = 0)$, to be transported from one bed to another one to realize the pressure swing. This situation is contrary to the cycle configurations DR-PL-A and DR-PH-A where one compressor can be utilized since the composition of different streams that need to be compressed is identical (pure A). Consequently, the capital cost of DR-PL-B and DR-PH-B units will be higher than that of DR-PL-A and DR-PH-A units.

6. CONCLUSIONS

The usefulness of an equilibrium theory-based mathematical model to simulate the perfect separation of binary feed gas mixture at CSS (cyclic steady state conditions) was formerly reported[20,22] for DR-PSA systems that accomplish pressure swing via heavy gas (DR-PL-A and DR-PH-A). This is further extended in this work to the DR-PSA systems that accomplish pressure swing via light gas (DR-PL-B and DR-PH-B). In particular, process design limitations required to accomplish complete separation of a two-components gas mixture at CSS in DR-PL-B and DR-PH-B cycle configurations are discussed. Triangular operating zone (TOZ), within which perfect separation at CSS can be realized is also identified. Such TOZ unambiguously links the unique value of Z_F (reported by Kearns and Webley[3]) to its minimum $(Z_{F,Min})$ and maximum $(Z_{F,Max})$ value (analogous to the suggestion of Ebner and Ritter[19]). Furthermore, a methodology to compute the optimum location for feed injection $\left(Z_{F,opt}\right)$ along with other pertinent operating settings is presented; here optimality refers to the maximum adsorbent utilization. However, since the hypotheses on which the equilibrium theory is based are not necessarily realized in practice, in real systems a complete separation can be not achieved even if the operating parameters are inside the range predicted by the equilibrium theory.

A thorough investigation of the influence of the process input parameters ($\mathbb{P}$, y_F and, β) on main operating settings ($\mathbb{G}$ and $Z_{F,opt}$), and an appropriate process selection criterion $\left(N_{F,Max}/N_{Comp}\right)$ is comparatively discussed for both

DOI: 10.1021/acs.iecr.8b04415

(DR-PL-B and DR-PH-B) process cycle configurations. Also proposed is an optimal operating pressure ratio range for all DR-PSA systems. Application of the selection criterion to facilitate the choice amongst all four DR-PSA process cycle configurations is finally demonstrated. Major inferences drawn from this study (equilibrium theory analysis restricted to complete separation at CSS) are:

(i) If shock forms (due to superposition of characteristics), it will initiate only at highest limiting concentration values in DR-PH-B and DR-PL-B process cycle configurations;

(ii) In DR-PL-B configuration, the feed position can essentially exist *almost* over the entire column length;

(iii) $Z_{F,opt}$ values decrease with increase in $\mathbb{P}$ in all DR-PSA process cycle configurations, but DR-PL-B (where $Z_{F,opt}$ values increase with increase in $\mathbb{P}$);

(iv) For pragmatic $Z_{F,opt}$ values, operate the DR-PL-B and DR-PH-B process at lower $\mathbb{P}$;

(v) In all DR-PSA process cycle configurations, higher recycle ratios are required for adsorbents with lower selectivity;

(vi) DR-PL-A and DR-PL-B systems should be chosen (over DR-PH-A and DR-PH-B, respectively) only when feed gas with very high values of y_F needs to be processed;

(vii) DR-PSA systems that accomplish pressure swing via pure light gas (DR-PL-B and DR-PH-B) are capable of processing higher quantity of feed gas at lower consumption of energy when compared with DR-PSA systems that accomplish pressure swing via pure heavy gas (DR-PL-A and DR-PH-A).

DOI: 10.1021/acs.iecr.8b04415

NOMENCLATURE

A	component that is strongly adsorbed, heavy species/ product
B	component that is weakly adsorbed, light species/ product
BD	process step: *blowdown*
$Bed-I$	adsorbent bed shown in Fig.1 and Fig.2
$Bed-II$	adsorbent bed shown in Fig.1 and Fig.2
$\mathbb{C}$	capacity ratio of the *purge* step, *dimensionless*
C	characteristic
CSS	cyclic steady state
$\mathbb{C}_{Max}$	maximum capacity ratio of the *purge* step, *dimensionless*
DR-PH-A	dual reflux pressure swing adsorption cycle with feed injection to the high pressure column and pressure swing via heavy gas
DR-PL-A	dual reflux pressure swing adsorption cycle with feed injection to the low pressure column and pressure swing via heavy gas
DR-PH-B	dual reflux pressure swing adsorption cycle with feed injection to the high pressure column and pressure swing via light gas
DR-PL-B	dual reflux pressure swing adsorption cycle with feed injection to the low pressure column and pressure swing via light gas
DR-PSA	dual reflux pressure swing adsorption
FE	process step: *feed*
$\mathbb{G}$	ratio of pure light reflux to feed rate, light recycle ratio, *dimensionless*
$\mathbb{H}$	dimensionless parameter defined via Eq.(21)
HP	heavy product
HR	heavy recycle
L_{bed}	adsorbent bed length, *m*
LP	light product
LR	light recycle
N	molar amount, *kmol*
$\dot{N}$	molar flowrate, *kmol/s*
N_{BD}	quantity of gas pushed-out of the adsorbent bed during *blowdown* step, *kmol*
N_{Comp}	quantity of gas that needs to be compressed, *kmol*
$N_{Comp,PS}$	actual quantity of gas that needs to be compressed to realize pressure swing, *kmol*
$\dot{N}_F$	feed flowrate, *kmol/s*
N_F	quantity of feed, *kmol*
$N_{F,Max}$	maximum quantity of feed gas that can be perfectly separated, *kmol*
$\dot{N}_{H,in}$	heavy recycle flowrate, *kmol/s*
$\dot{N}_{H,out}$	flowrate of gas pushed-out of the adsorbent bed operated at constant high pressure, *kmol/s*
$\dot{N}_{L,in}$	light recycle flowrate, *kmol/s*
$\dot{N}_{L,out}$	flowrate of gas pushed-out of the adsorbent bed operated at constant low pressure, *kmol/s*
N_{PR}	quantity of gas injected-in the adsorbent bed undergoing pressurization step, *kmol*
$\dot{N}_{RS,in}$	flowrate of gas injected-in the *rectifying section* of the bed, *kmol/s*
$\dot{N}_{RS,out}$	flowrate of gas pushed-out of the *rectifying section* of the bed, *kmol/s*
$\dot{N}_{SS,in}$	flowrate of gas injected-in the *stripping section* of the bed, *kmol/s*
$\dot{N}_{SS,out}$	flowrate of gas pushed-out of the *stripping section* of the bed, *kmol/s*
$\mathbb{P}$	ratio of high operating pressure to low operating pressure (operating pressure ratio), *dimensionless*
P	final pressure, total pressure, *bar*
P_0	initial pressure, *bar*
P_{Eq}	pressure at the end of the equalization step assumed to be equivalent to: $(P_H + P_L)/2$, *bar*
P_H	high pressure, *bar*
P_L	low pressure, *bar*
PR	process step: *pressurization*
PSA	pressure swing adsorption
PU	process step: *purge*

DOI: 10.1021/acs.iecr.8b04415

R	ideal gas constant, *(m^3.bar)/(K.kmol)*
RS	*rectifying section*
RW	rectifying wave
S	shock
SS	*stripping section*
SW	stripping wave
T	temperature, *K*
t	time, *s*
t_{cycle}	cycle duration, *s*
t_{FE}	*feed* step duration, *s*
TOZ	triangular operating zone
t_{PU}	*purge* step duration, *s*
t_{step}	step duration, *s*
V_{bed}	volume of adsorbent bed, *m^3*
y	final concentration in terms of A, or specific concentration in terms of A, mole fraction of heavy species, *dimensionless*
$(1-y)$	mole fraction of light species, *dimensionless*
$\mathbb{Y}(y)$	dimensionless parameter equal to: $1+(\beta-1)y$
$(y=0)$	mole fraction of pure light gas, *dimensionless*
$(y=1)$	mole fraction of pure heavy gas, *dimensionless*
y_0	initial composition in terms of A, *dimensionless*
y_1	composition at a specific location in terms of A, mole fraction of heavy species at the leading edge of the shock wave, *dimensionless*
y_2	composition at a specific location in terms of A, mole fraction of heavy species at the trailing edge of the shock wave, *dimensionless*
y_F	mole fraction of heavy species in binary feed gas mixture, *dimensionless*
y^*	explicit mole fraction in terms of A, *dimensionless*
Z	axial co-ordinate normalized with respect to bed length, final location, *dimensionless*
z	location along the length of the adsorbent bed, *m*
$Z=0$	adsorbent bed end (pure heavy gas is either fed at this end or is pushed-out from this end), *dimensionless*
$Z=1$	adsorbent bed end (pure light gas is either fed at this end or is pushed-out from this end), *dimensionless*
Z_0	initial location, *dimensionless*
Z_F	location where binary feed gas mixture is injected-in the adsorbent bed, *dimensionless*
$Z_{F,Max}$	maximum limit of the location where binary feed gas mixture can be injected-in the adsorbent bed, *dimensionless*
$Z_{F,Min}$	minimum limit of the location where binary feed gas mixture can be injected-in the adsorbent bed, *dimensionless*
$Z_{F,opt}$	optimum location where binary feed gas mixture should be injected-in the adsorbent bed, *dimensionless*

Greek letters

β	adsorbent separation parameter equivalent to: (β_A/β_B), *dimensionless*
β_i	adsorbent separation parameter for component i, *dimensionless*
ε	adsorbent bed's interstitial porosity, *dimensionless*
θ	time co-ordinate normalized with respect to the duration of a process step, *dimensionless*

Subscripts

0	initial location or condition, pure light gas concentration
$1,2$	composition of gas in terms of A at the leading and trailing edge of the shock wave, respectively; composition of gas in terms of A at a specific location
A	strongly adsorbed species, heavy component

DOI: 10.1021/acs.iecr.8b04415

B	weakly adsorbed species, light component
BD	process step: *blowdown*
bed	adsorbent bed
C	characteristic
$Comp$	quantity of gas that needs to be compressed
$Comp, PS$	quantity of gas that needs to be compressed to accomplish pressure swing
Eq	pressure at the end of equalization step
F	concentration of A in binary feed gas mixture, location where feed is supplied to the bed, molar flowrate of feed gas, molar quantity of feed gas
F, Max	maximum quantity of feed gas that can be perfectly separated
FE	Process step: *feed*
H	high pressure
H, in	pure heavy recycle
H, out	gas pushed-out of the adsorbent bed operational at constant high pressure
L	low pressure
L, in	pure light recycle
L, out	gas pushed-out of the adsorbent bed operational at constant low pressure
Max	maximum
Min	minimum
opt	optimum
PR	process step: *pressurization*
PU	process step: *purge*
RS	*rectifying section*
RS, in	gas injected-in the *rectifying* section of the bed
RS, out	gas pushed-out of the *rectifying* section of the bed
RW	*rectifying* wave
S	shock wave
SS	*stripping* section
SS, in	gas injected-in the *stripping* section of the bed
SS, out	gas pushed-out of the *stripping* section of the bed
$step$	process step
SW	*stripping* wave

Superscripts

FE, BD, PU, PR	positions at the termination of *feed, blowdown*, *purge and, pressurization*, respectively
$*$	concentration of gas at leading or trailing edge of a shock, concentration of a characteristic in terms of A, specific location

DOI: 10.1021/acs.iecr.8b04415

ASSOCIATED CONTENT

Supporting Information

The Supporting Information is available free of charge on the ACS Publications Website at DOI:

EQUILIBRIUM MODEL AND OPTIMAL SOLUTION FOR DR-PL-B PROCESS CYCLE CONFIGURATION; NUMERICAL SOLUTION; UTILIZATION OF THE TRIANGULAR OPERATING ZONE FOR DEMONSTRATION OF THE OPTIMUM DESIGN APPROACH; DR-PH-B process cycle configuration: Triangular Operating Zone (TOZ) for $(y_F = 0.5)$, $(\beta = 0.5)$ and $(\mathbb{P} = 1.5)$ (Figure S1); DR-PH-B process cycle configuration: Composition profiles for *Test-A* depicted in Triangular Operating Zone (TOZ of Figure S1) (Figure S2); DR-PH-B process cycle configuration: Composition profiles for *Test-B* depicted in Triangular Operating Zone (TOZ of Figure S1). The shaded portion represents the unutilized region of the bed (Figure S3); DR-PH-B process cycle configuration: Composition profiles for *Test-C* depicted in Triangular Operating Zone (TOZ of Figure S1). The shaded portion represents the unutilized region of the bed (Figure S4); DR-PH-B process cycle configuration: Composition profiles for *Test-D* depicted in Triangular Operating Zone (TOZ of Figure S1). The shaded portions represent the unutilized regions of the bed (Figure S5); DR-PL-B process cycle configuration: Triangular Operating Zone (TOZ) for $(y_F = 0.5)$, $(\beta = 0.5)$ and $(\mathbb{P} = 1.5)$ (Figure S6); DR-PL-B process cycle configuration: Composition profiles for *Test-A* depicted in Triangular Operating Zone (TOZ of Figure S6) (Figure S7); DR-PL-B process cycle configuration: Composition profiles for *Test-B* depicted in Triangular Operating Zone (TOZ of Figure S6). The shaded portion represents the unutilized region of the bed (Figure S8); DR-PL-B process cycle configuration: Composition profiles for *Test-C* depicted in Triangular Operating Zone (TOZ of Figure S6). The shaded portion represents the unutilized region of the bed (Figure S9); DR-PL-B process cycle configuration: Composition profiles for *Test-D* depicted in Triangular Operating Zone (TOZ of Figure S6). The shaded portion represents the unutilized region of the bed (Figure S10).

DOI: 10.1021/acs.iecr.8b04415

REFERENCES

(1) Hirose, T., 1991. A simple design method of a new PSA process consisting of both rectifying and stripping sections. In Proceedings of the 2nd China-Japan-USA Symposium on Adsorption (Vol. 123).

(2) Leavitt, F.W., Union Carbide Industrial Gases Technology Corporation, 1992. Duplex adsorption process. U.S. Patent 5,085,674.

(3) Kearns, D.T. and Webley, P.A., 2006A. Modelling and evaluation of dual-reflux pressure swing adsorption cycles: Part I. Mathematical models. Chemical engineering science, 61(22), pp.7223-7233.

(4) Diagne, D., Goto, M. and Hirose, T., 1994. New PSA process with intermediate feed inlet position operated with dual refluxes: application to carbon dioxide removal and enrichment. Journal of chemical engineering of Japan, 27(1), pp.85-89.

(5) Diagne, D., Goto, M. and Hirose, T., 1995. Experimental study of simultaneous removal and concentration of CO 2 by an improved pressure swing adsorption process. Energy conversion and management, 36(6), pp.431-434.

(6) Diagne, D., Goto, M. and Hirose, T., 1995. Parametric studies on CO2 separation and recovery by a dual reflux PSA process consisting of both rectifying and stripping sections. Industrial & engineering chemistry research, 34(9), pp.3083-3089.

(7) Mc Intyre, J.A., Holland, C.E. and Ritter, J.A., 2002. High enrichment and recovery of dilute hydrocarbons by dual-reflux pressure-swing adsorption. Industrial & engineering chemistry research, 41(14), pp.3499-3504.

(8) McIntyre, J.A., Ebner, A.D. and Ritter, J.A., 2010. Experimental study of a dual reflux enriching pressure swing adsorption process for concentrating dilute feed streams. Industrial & Engineering Chemistry Research, 49(4), pp.1848-1858.

(9) Bhatt, T.S., Sliepcevich, A., Storti, G. and Rota, R., 2014. Experimental and modeling analysis of dual-reflux pressure swing adsorption process. Industrial & Engineering Chemistry Research, 53(34), pp.13448-13458.

(10) Saleman, T.L., Li, G.K., Rufford, T.E., Stanwix, P.L., Chan, K.I., Huang, S.H. and May, E.F., 2015. Capture of low grade methane from nitrogen gas using dual-reflux pressure swing adsorption. Chemical Engineering Journal, 281, pp.739-748.

(11) Li, D., Zhou, Y., Shen, Y., Sun, W., Fu, Q., Yan, H. and Zhang, D., 2016. Experiment and simulation for separating CO 2/N 2 by dual-reflux pressure swing adsorption process. Chemical Engineering Journal, 297, pp.315-324.

(12) Diagne, D., Goto, M. and Hirose, T., 1996. Numerical analysis of a dual refluxed PSA process during simultaneous removal and concentration of carbon dioxide dilute gas from air. Journal of Chemical Technology and Biotechnology, 65(1), pp.29-38.

(13) Spoorthi, G., Thakur, R.S., Kaistha, N. and Rao, D.P., 2011. Process intensification in PSA processes for upgrading synthetic landfill and lean natural gases. Adsorption, 17(1), pp.121-133.

(14) Thakur, R.S., Kaistha, N. and Rao, D.P., 2011. Process intensification in duplex pressure swing adsorption. Computers & Chemical Engineering, 35(5), pp.973-983.

(15) Sivakumar, S.V. and Rao, D.P., 2011. Modified Duplex PSA. 1. Sharp separation and process intensification for CO2- N2- 13X zeolite system. Industrial & Engineering Chemistry Research, 50(6), pp.3426-3436.

(16) Sivakumar, S.V. and Rao, D.P., 2011. Modified Duplex PSA. 2. Sharp separation and process intensification for N2-O2-5A zeolite system. Industrial & Engineering Chemistry Research, 50(6), pp.3437-3445.

(17) Bhatt, T.S., Storti, G. and Rota, R., 2015. Detailed simulation of dual-reflux pressure swing adsorption process. Chemical Engineering Science, 122, pp.34-52.

(18) Zhang, Y., Saleman, T.L., Li, G.K., Xiao, G., Young, B.R. and May, E.F., 2016. Non-isothermal numerical simulations of dual reflux pressure swing adsorption cycles for separating N 2+ CH 4. Chemical Engineering Journal, 292, pp.366-381.

(19) Ebner, A.D. and Ritter, J.A., 2004. Equilibrium theory analysis of dual reflux PSA for separation of a binary mixture. AIChE journal, 50(10), pp.2418-2429.

(20) Bhatt, T.S., Storti, G. and Rota, R., 2013. Optimal design of dual-reflux pressure swing adsorption units via equilibrium theory. Chemical Engineering Science, 102, pp.42-55.

(21) Kearns, D.T. and Webley, P.A., 2006B. Modelling and evaluation of dual reflux pressure swing adsorption cycles: Part II. Productivity and energy consumption. Chemical engineering science, 61(22), pp.7234-7239.

(22) Bhatt, T.S., Storti, G., Denayer, J.F. and Rota, R., 2017. Optimal design of dual-reflux pressure swing adsorption units via equilibrium theory: Process configurations employing heavy gas for pressure swing. Chemical Engineering Journal, 311, pp.385-406.

(23) Tian, C., Fu, Q., Ding, Z., Han, Z. and Zhang, D., 2017. Experiment and simulation study of a dual-reflux pressure swing adsorption process for separating N2/O2. Separation and Purification Technology, 189, pp.54-65.

(24) Shen, Y., Zhou, Y., Li, D., Fu, Q., Zhang, D. and Na, P., 2017. Dual-reflux pressure swing adsorption process for carbon dioxide capture from dry flue gas. International Journal of Greenhouse Gas Control, 65, pp.55-64.

DOI: 10.1021/acs.iecr.8b04415

(25) May, E.F., Zhang, Y., Saleman, T.L., Xiao, G., Li, G.K. and Young, B.R., 2017. Demonstration and optimisation of the four Dual-Reflux Pressure Swing Adsorption configurations. Separation and Purification Technology, 177, pp.161-175.
(26) Zou, Y., Xiao, G., Li, G., Lu, W. and May, E.F., 2017. Advanced non-isothermal dynamic simulations of dual reflux pressure swing adsorption cycles. Chemical Engineering Research and Design, 126, pp.76-88.
(27) Kim, S., Ko, D. and Moon, I., 2016. Dynamic Optimization of a Dual Pressure Swing Adsorption Process for Natural Gas Purification and Carbon Capture. Industrial & Engineering Chemistry Research, 55(48), pp.12444-12451.
(28) Khurana, M. and Farooq, S., 2016. Simulation and optimization of a 6-step dual-reflux VSA cycle for post-combustion CO 2 capture. Chemical Engineering Science, 152, pp.507-515.
(29) LI, G., May, E.F., Webley, P.A., Huang, S.H.W. and Chan, K.I., THE UNIVERSITY OF WESTERN AUSTRALIA and CHEVRON USA INC., 2017. METHOD FOR GAS SEPARATION. U.S. Patent 20,170,348,670.
(30) Rhee, H.K.; Aris R.; Amundson N.R. First-order partial differential equations, Prentice-Hall 1986, Vol. 1, Englewood Cliffs, NJ.

DOI: 10.1021/acs.iecr.8b04415

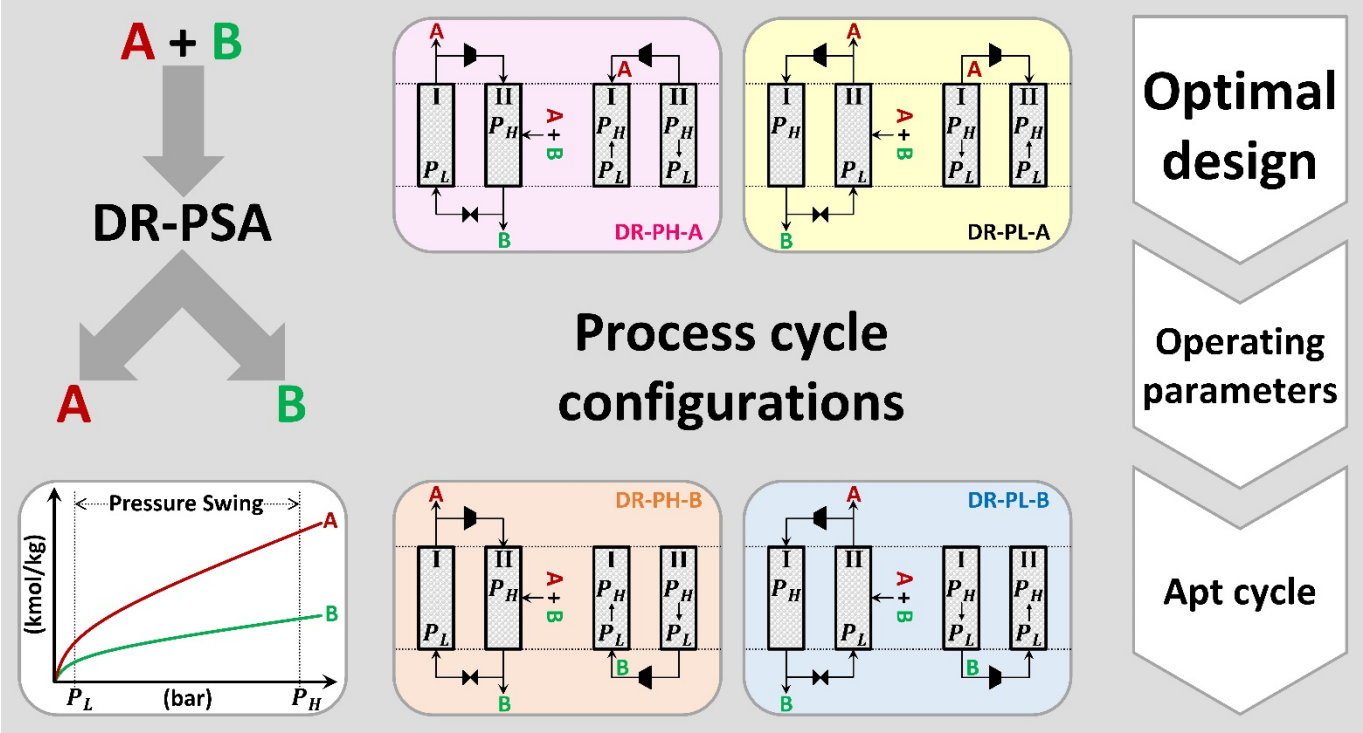

Abstract Graphics

DOI: 10.1021/acs.iecr.8b04415

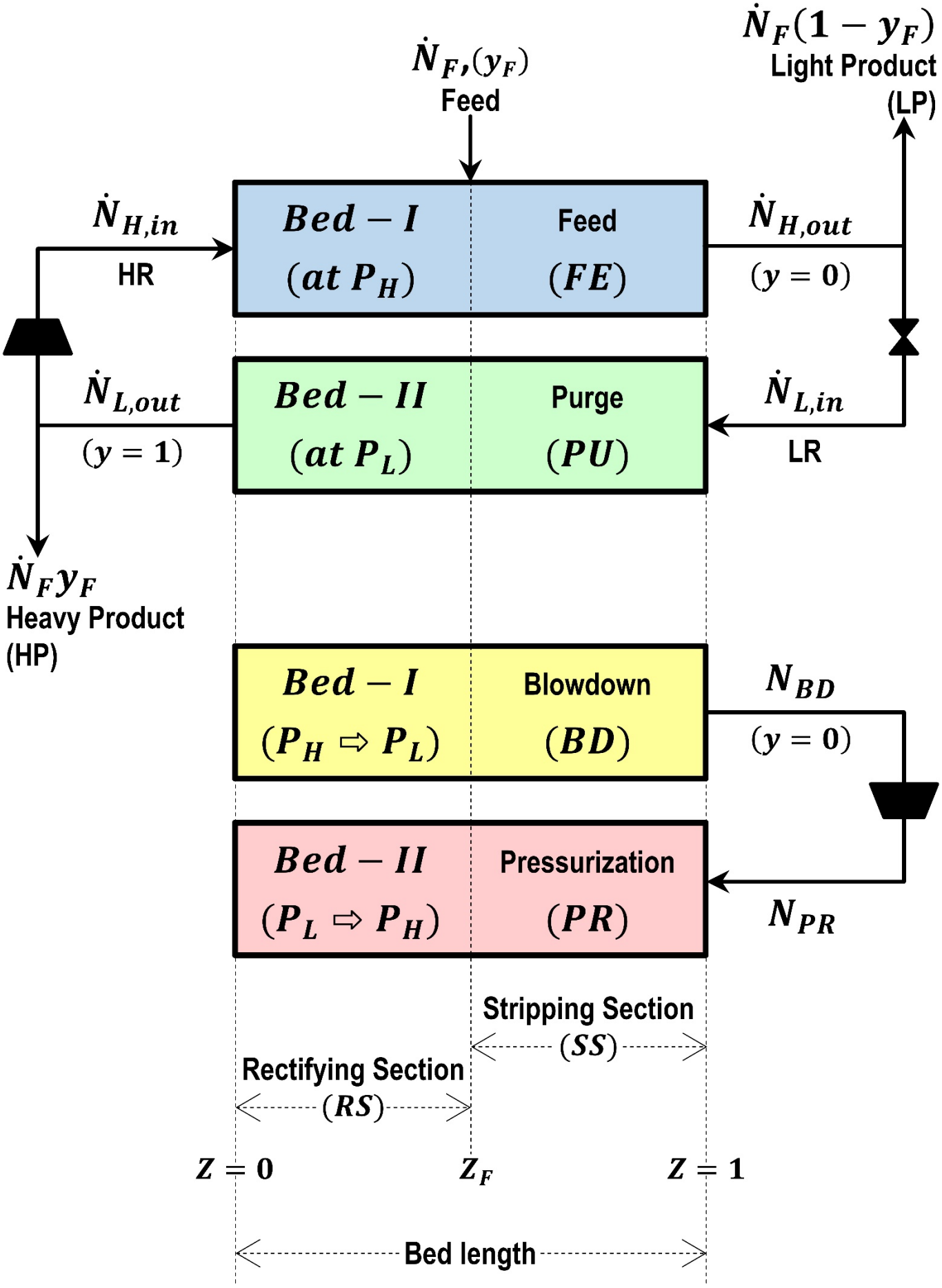

Fig. 1. Cycle steps and flows of a typical DR-PH-B process cycle configuration for complete separation at *CSS*.

DOI: 10.1021/acs.iecr.8b04415

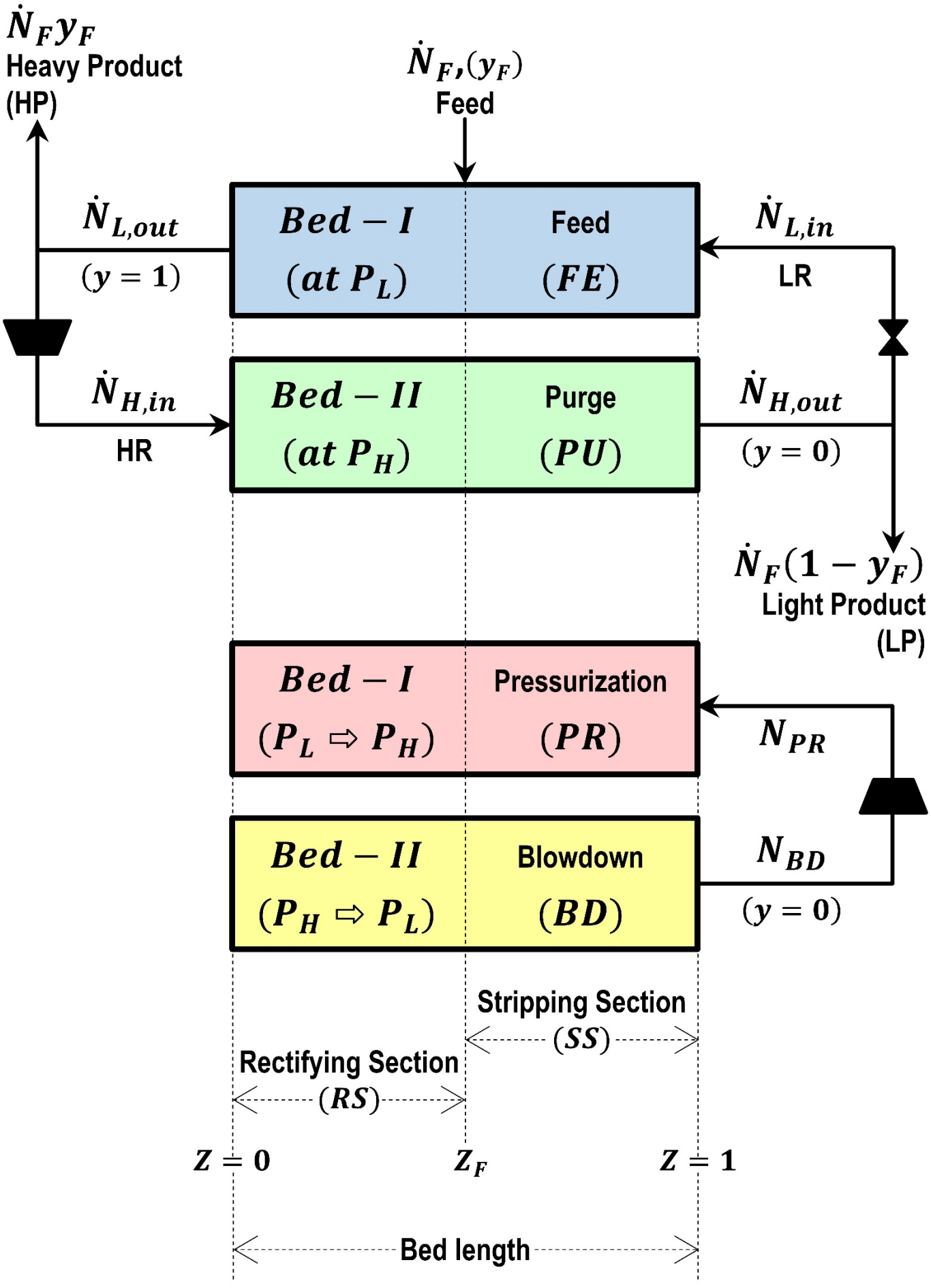

Fig. 2. Cycle steps and flows of a typical DR-PL-B process cycle configuration for complete separation at *CSS*.

DOI: 10.1021/acs.iecr.8b04415

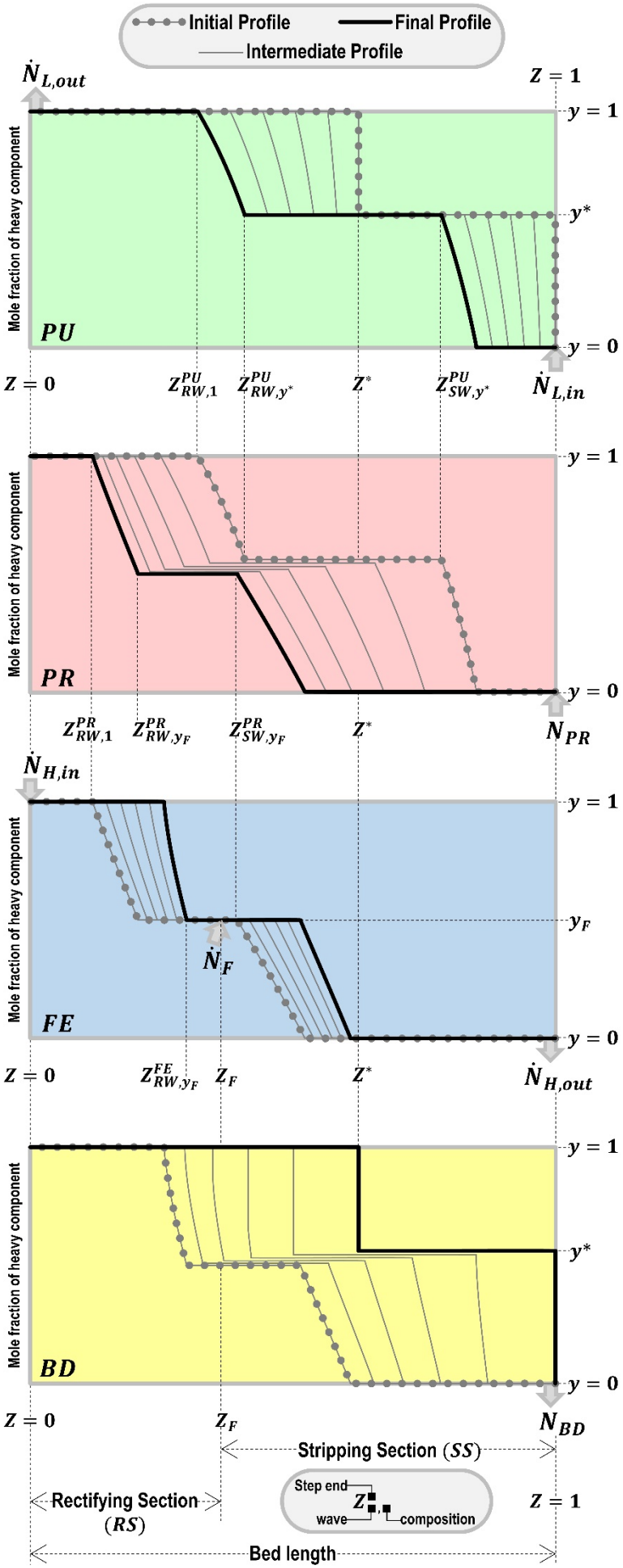

Fig. 3. Composition profiles for DR-PH-B process cycle configuration during the four steps of the cyclic process, for complete separation at CSS.

DOI: 10.1021/acs.iecr.8b04415

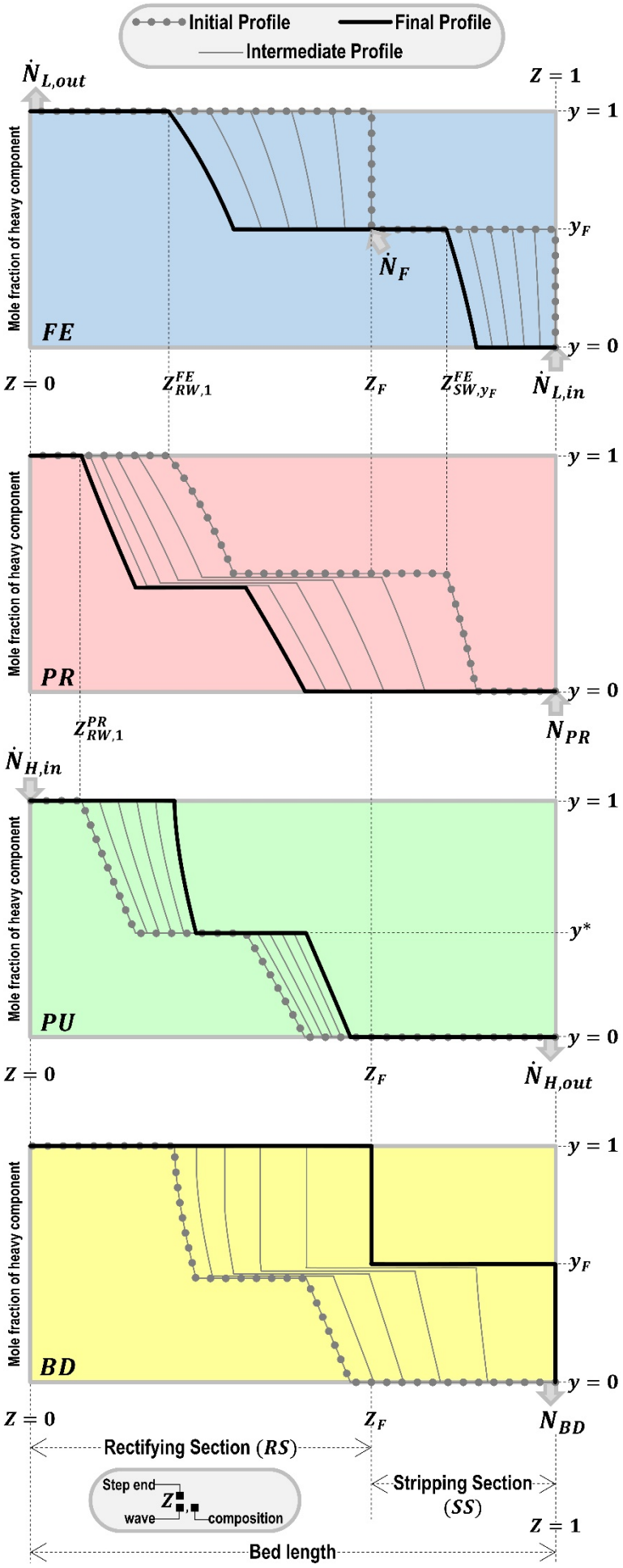

Fig. 4. Composition profiles for DR-PL-B process cycle configuration during the four steps of the cyclic process, for complete separation at CSS.

DOI: 10.1021/acs.iecr.8b04415

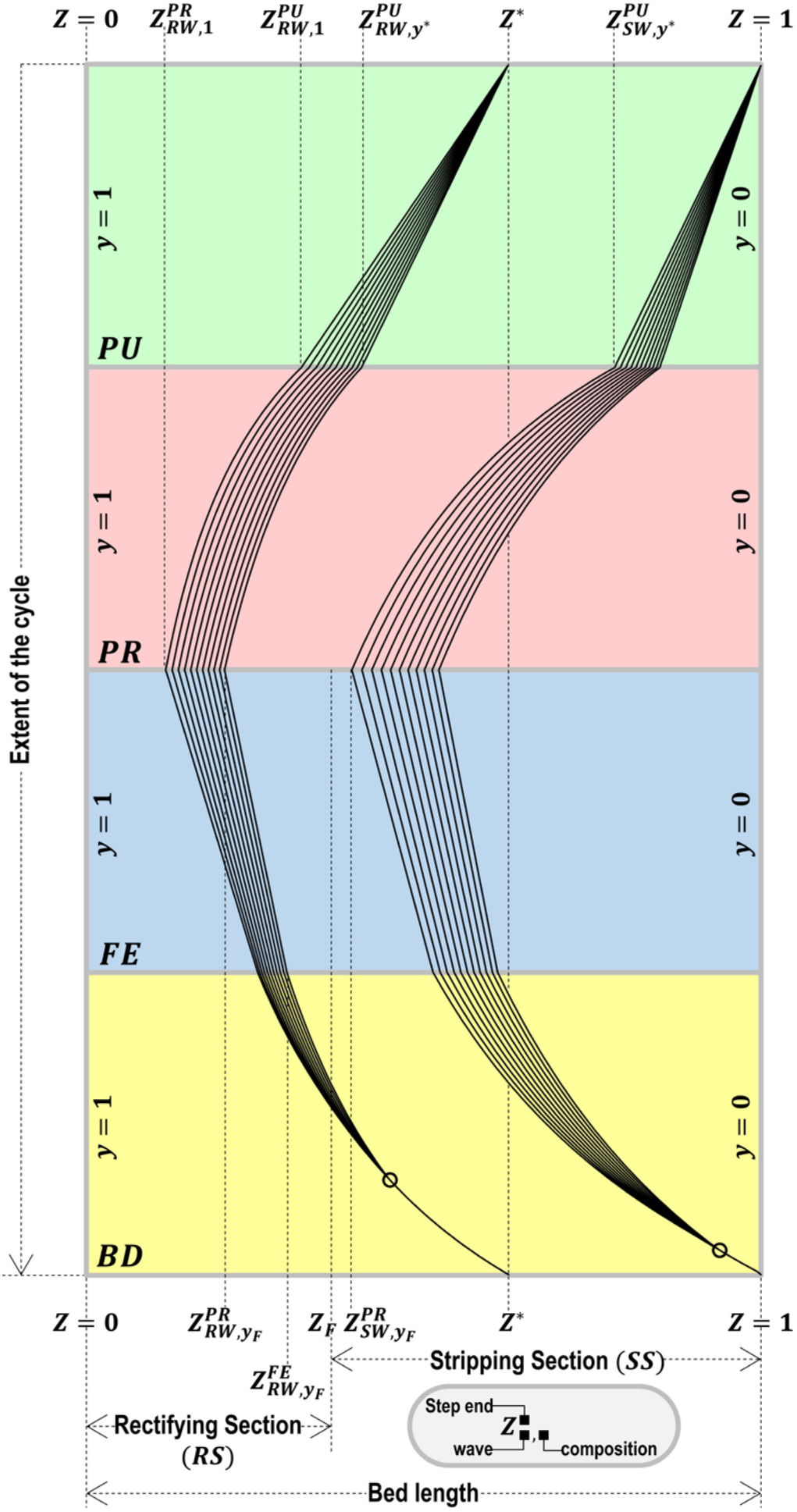

Fig. 5. Trajectory of waves/shocks in both sections of a column for DR-PH-B process cycle configuration during the four steps of the cyclic process, for complete separation at CSS.

DOI: 10.1021/acs.iecr.8b04415

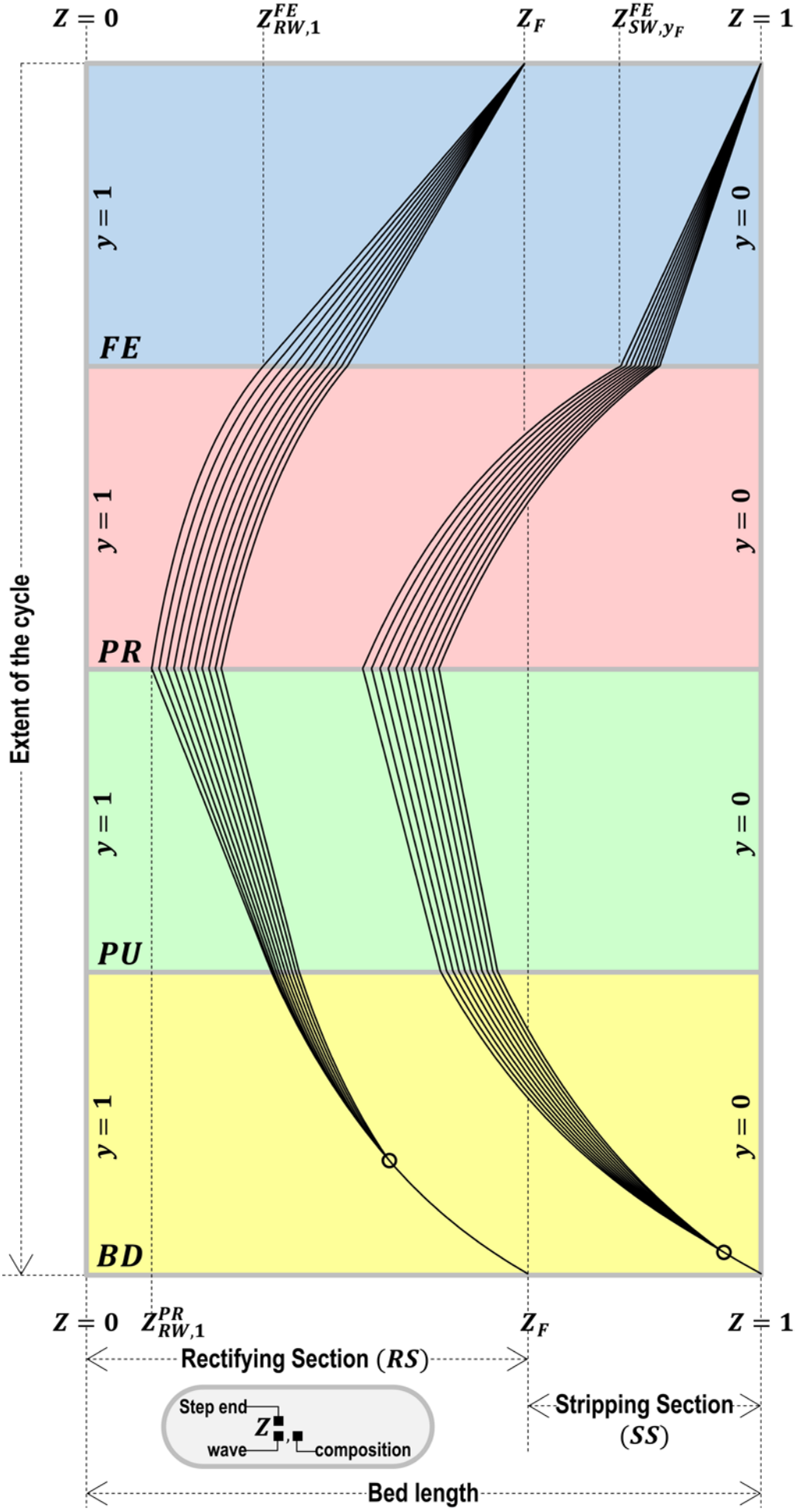

Fig. 6. Trajectory of waves/shocks in both sections of a column for DR-PL-B process cycle configuration during the four steps of the cyclic process, for complete separation at CSS.

DOI: 10.1021/acs.iecr.8b04415

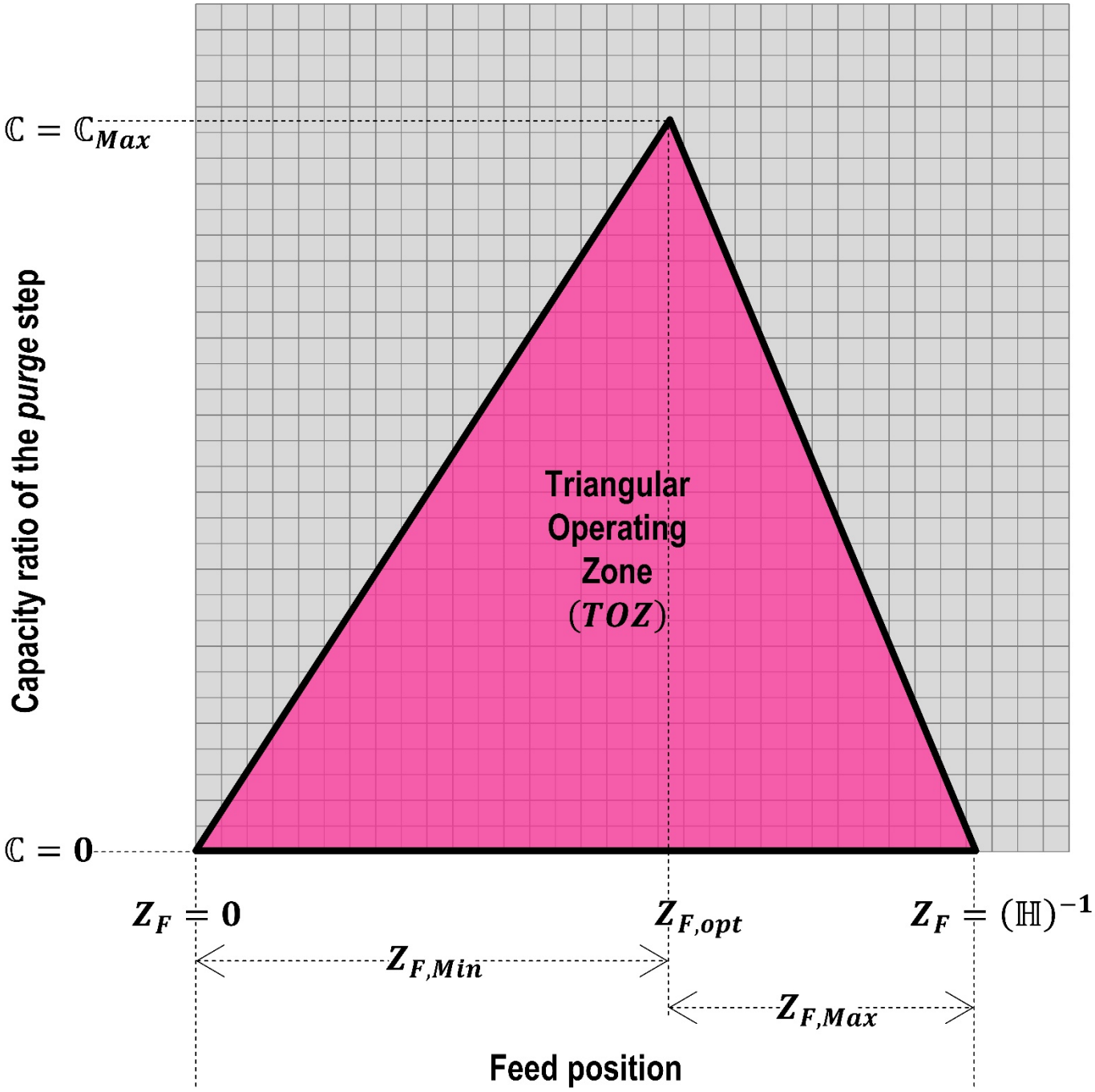

Fig. 7. Qualitative representation of 'Triangular Operating Zone' for DR-PH-B process cycle configuration.

DOI: 10.1021/acs.iecr.8b04415

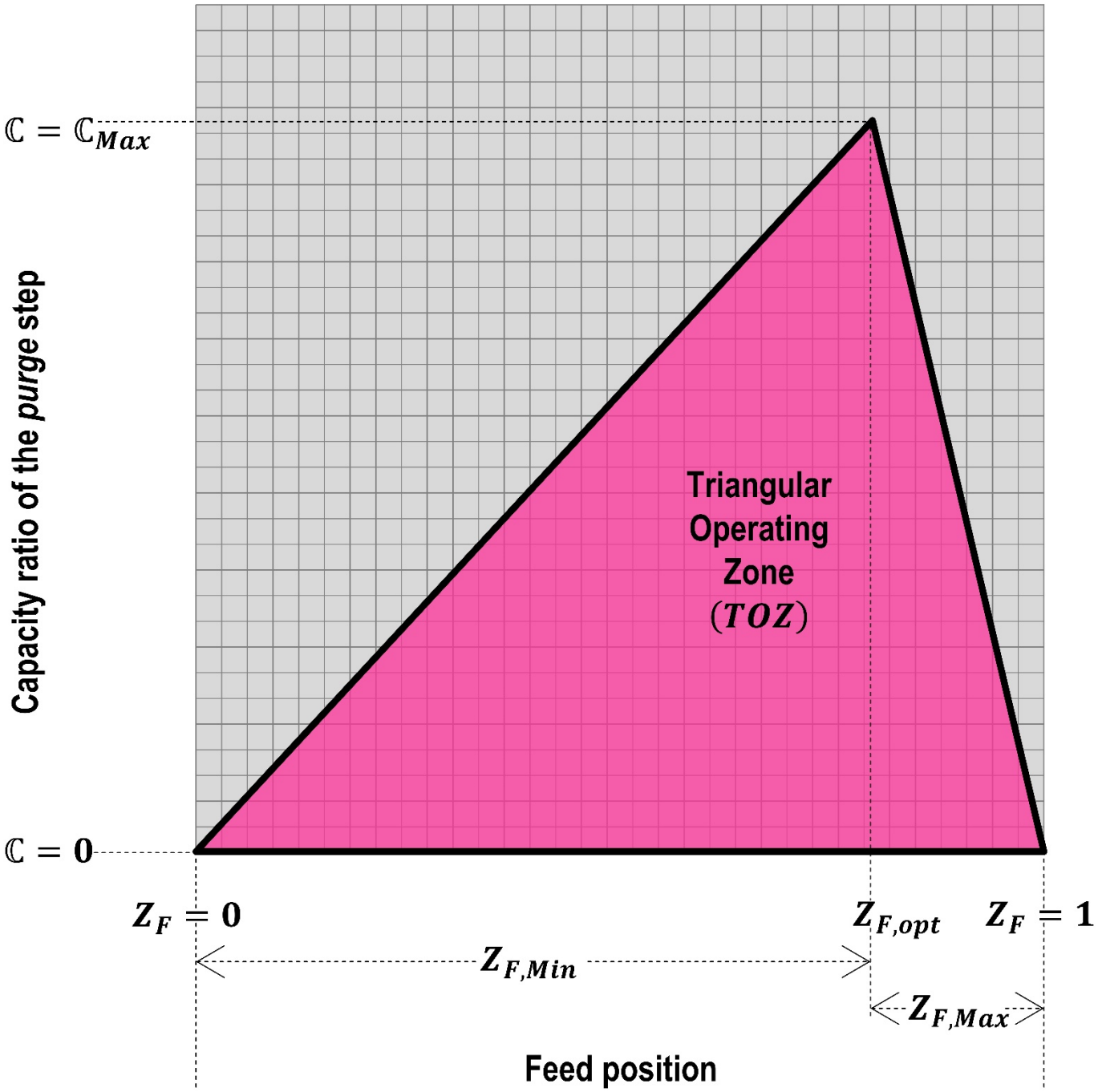

Fig. 8. Qualitative representation of 'Triangular Operating Zone' for DR-PL-B process cycle configuration.

DOI: 10.1021/acs.iecr.8b04415

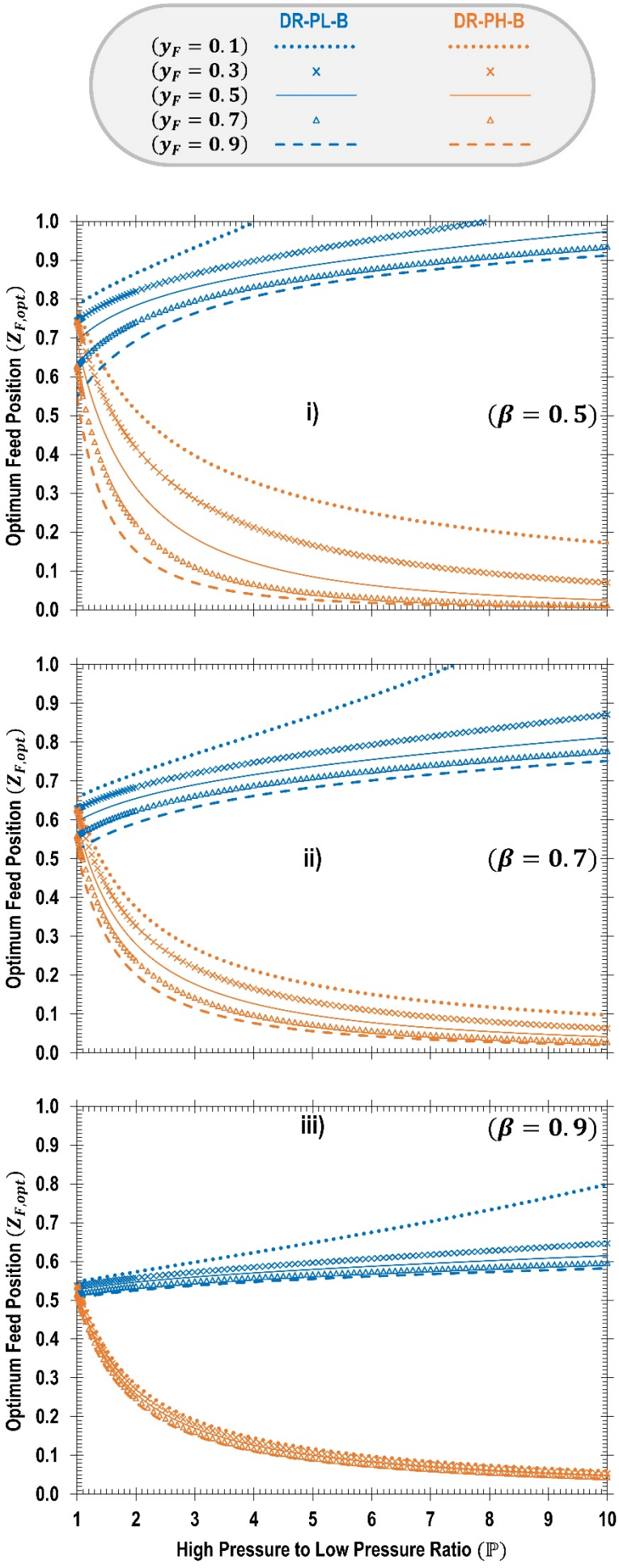

Fig. 9. $\mathbb{P}$ versus $Z_{F,opt}$ in DR-PH-B and DR-PL-B process cycle configurations, for: β equal to 0.5, 0.7 and 0.9 and; y_F equal to 0.1, 0.3, 0.5, 0.7 and 0.9.

DOI: 10.1021/acs.iecr.8b04415

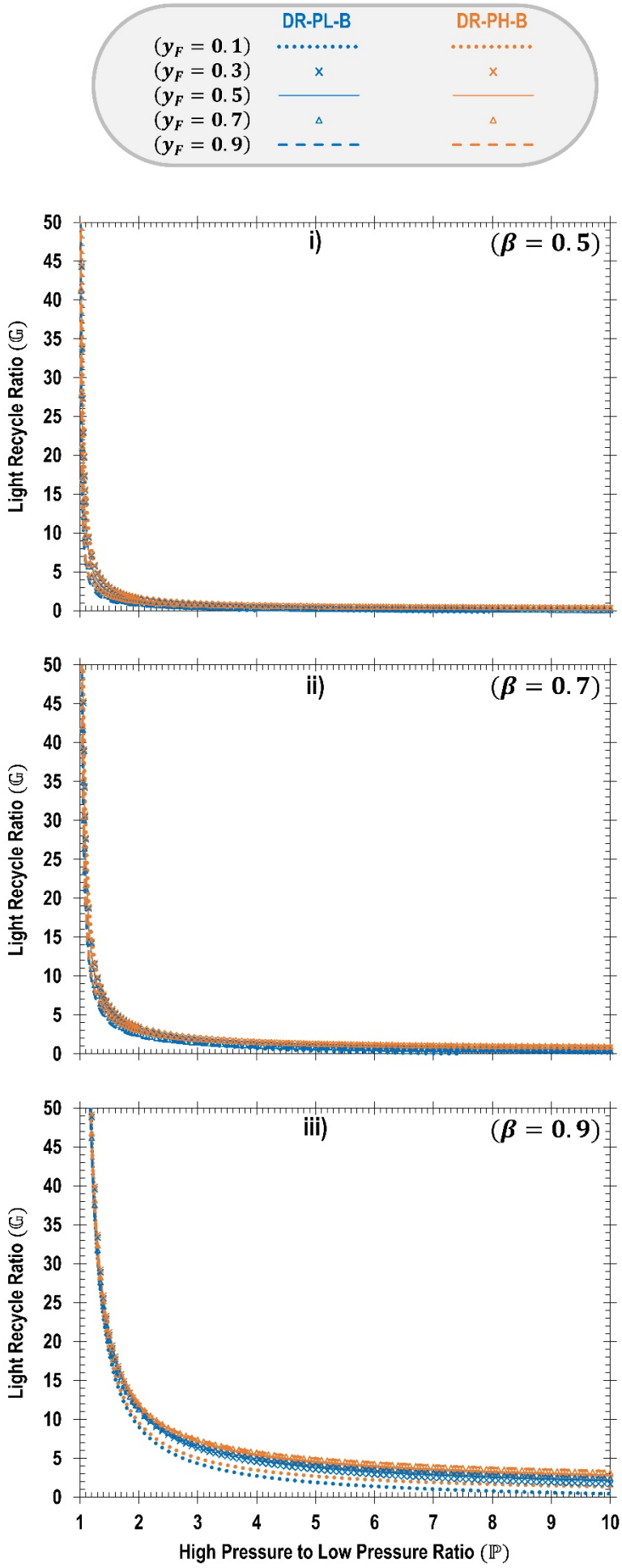

Fig. 10. $\mathbb{P}$ versus $\mathbb{G}$ in DR-PH-B and DR-PL-B process cycle configurations, for: β equal to 0.5, 0.7 and 0.9 and; y_F equal to 0.1, 0.3, 0.5, 0.7 and 0.9.

DOI: 10.1021/acs.iecr.8b04415

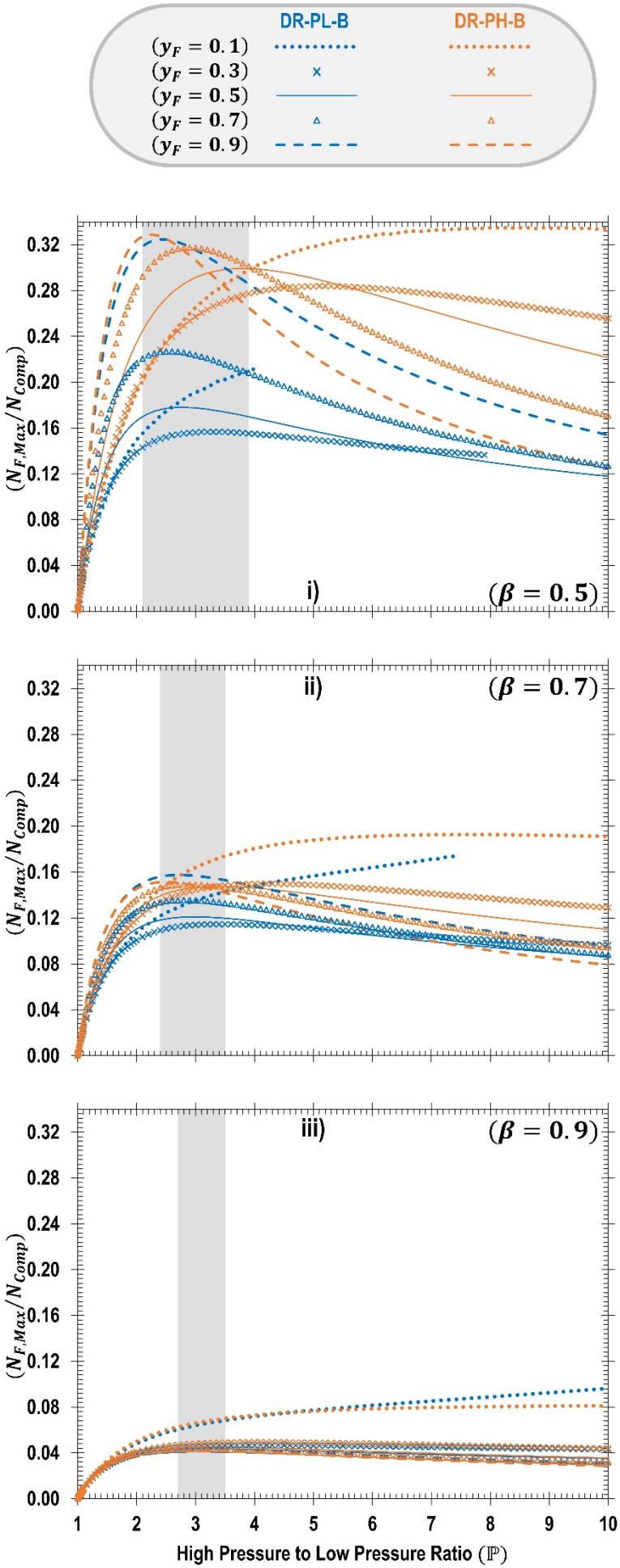

Fig. 11. $\mathbb{P}$ versus $N_{F,Max}/N_{Comp}$ in DR-PH-B and DR-PL-B process cycle configurations, for: β equal to 0.5, 0.7 and 0.9 and; y_F equal to 0.1, 0.3, 0.5, 0.7 and 0.9. The shaded regions represent the optimal high to low operating pressure ratio range (neglecting y_F equal to 0.1 and 0.3).

DOI: 10.1021/acs.iecr.8b04415